

A hybrid kinetic and constraint-based model of leaf metabolism allows predictions of metabolic fluxes in different environments

Sanu Shameer^{1,†}, Yu Wang^{2,†}, Pedro Bota¹, R. George Ratcliffe¹, Stephen P. Long^{2,3}, Lee J. Sweetlove¹

¹ Department of Plant Sciences, University of Oxford, South Parks Road, Oxford OX1 3RB, UK

² Carl R Woese Institute for Genomic Biology, University of Illinois at Urbana-Champaign, Urbana, IL, 61801, USA

³ Lancaster Environment Centre, Lancaster University, Lancaster, LA1 4YQ, UK

[†]These authors contributed equally to this work.

Abstract

While flux balance analysis (FBA) provides a framework for predicting steady-state leaf metabolic network fluxes, it does not readily capture the response to environmental variables without being coupled to other modelling formulations. To address this, we coupled an FBA model of 903 reactions of soybean (*Glycine max*) leaf metabolism with e-photosynthesis, a dynamic model that captures the kinetics of 130 reactions of photosynthesis and associated chloroplast carbon metabolism. Successful coupling was achieved in an iterative formulation in which fluxes from e-photosynthesis were used to constrain the FBA model and then, in turn, fluxes computed from the FBA model used to update parameters in e-photosynthesis. This process was repeated until common fluxes in the two models converged. Coupling did not hamper the ability of the kinetic module to accurately predict the carbon assimilation rate, photosystem II electron flux, and starch accumulation of field-grown soybean at two CO₂ concentrations. The coupled model also allowed accurate predictions of new parameters such as nocturnal respiration, as well as analysis of the effect of light intensity and elevated CO₂ on leaf metabolism. Predictions included an unexpected decrease in the rate of export of sucrose from the leaf at high light, due to altered starch-sucrose partitioning, and altered daytime flux modes in the TCA cycle at elevated CO₂. Mitochondrial fluxes were notably different between growing and mature leaves, with greater anaplerotic, TCA cycle and mitochondrial ATP synthase fluxes predicted in the former, primarily to provide carbon skeletons and energy for protein synthesis.

Keywords: (up to 10 keywords, listed in order of importance)

Metabolic modelling; flux balance analysis; kinetic modelling; Glycine max; central carbon metabolism.

Significance statement: (the statement should consist of up to two sentences of no more than 75 words in total and should not repeat the title)

A model of the relationship between photosynthesis and other metabolic pathways in soybean leaves was constructed by coupling a kinetic model of photosynthesis with a constraint-based stoichiometric model of the rest of leaf metabolism. The new modelling formulation allows a broad prediction of leaf metabolic behaviour under different environments and will be a useful tool for guiding strategies for improving leaf carbon and energy-use efficiency.

Introduction

Improving the efficiency of photosynthesis has been proposed as a feasible, and underexploited, means to increase crop yield (Zhu *et al.*, 2010, Long *et al.*, 2019). Recent attempts to engineer increased photosynthetic rates have resulted in improved crop productivity in field trials, providing a test-of-concept (Kromdijk *et al.*, 2016, South *et al.*, 2019, López-Calcagno *et al.*, 2020, Yoon *et al.*, 2020). Despite these attempts, the photosynthetic energy conversion efficiency (ϵ_c , the fraction of intercepted radiation converted into plant mass) of current improvements is still far from the theoretical maximum (Zhu *et al.*, 2008, Zhu *et al.*, 2010, Long *et al.*, 2019). Successful intervention to increase ϵ_c depends on our understanding of the biochemical limitations of photosynthetic energy conversion. This is challenging because photosynthesis is directly or indirectly affected by other metabolic pathways (Paul and Foyer, 2001, Paul and Pellny, 2003).

Mathematical modelling is a powerful approach for understanding the photosynthetic process. Farquhar *et al.* (1980) developed a steady-state model of C_3 photosynthesis, which assumes photosynthesis cannot proceed faster than the limit set by the carboxylase activity or the electron transport rate. This model has been used to predict steady-state CO_2 assimilation rates and has proved robust under various environmental conditions, including light intensity, $[CO_2]$ and $[O_2]$. The Farquhar model and its later versions has been extensively used in other models of leaf metabolism (Caemmerer 2000, Yin and Struik 2009, Heckmann *et al.*, 2013). It is also commonly implemented as a submodule in multi-scale models such as crop growth models and land surface exchange models (Sellers *et al.*, 1996, Cox *et al.*, 1999, Miguez *et al.*, 2009, Vos *et al.*, 2010). However, the Farquhar model does not describe the individual metabolic reactions of photosynthesis, and so it cannot be used directly to study the fluxes through the leaf metabolic network or the impact of manipulating individual photosynthetic enzymes on the efficiency of the whole system. For insights into these processes, it is necessary to turn to other metabolic modelling approaches, such as constraint-based modelling and kinetic modelling.

Constraint-based modelling is a metabolic modelling approach that uses a set of physical, biochemical and thermodynamic constraints to define a solution space that describes all feasible flux distributions supported by a system of metabolic reactions of defined stoichiometry. This modelling approach does not require enzyme/metabolite concentrations or kinetic parameters (Beard and Qian, 2005). The most commonly implemented formulation - flux balance analysis (FBA) - has been extensively used to study leaf metabolism in C_3 plants (de Oliveira Dal'Molin *et al.*, 2010, Mintz-Oron *et al.*, 2012, Poolman *et al.*, 2013, Cheung *et al.*, 2014, Arnold and Nikoloski 2014, Cheung *et al.*, 2015, Lakshmanan *et al.*, 2015, Yuan *et al.*, 2016, Chatterjee *et al.*, 2017, Shameer *et al.*, 2019, Herrmann *et al.*, 2019). FBA is capable of modelling steady-state metabolic fluxes in stoichiometric models (Orth *et al.*, 2010) and current FBA leaf models are capable of modelling photosynthesis in growing and fully-expanded leaves. It is possible to include both daytime and night-time metabolism in the model, providing a more accurate description of leaf metabolism over the diel cycle (Cheung *et al.*, 2014, Töpfer *et al.*, 2020).

FBA models are based on reaction stoichiometries and require only a few biochemical and thermodynamic constraints. As a result, these models can be used to simulate flux distributions through extremely large metabolic networks, even genome-scale metabolic networks composed of more than 8000 reactions and metabolites in a computationally efficient manner (Simons *et al.*, 2014). FBA models are composed of entirely linear equations and while this makes them computationally efficient, most biological processes are non-linear and FBA models are unable to directly represent these non-linear processes. This makes it difficult to account for the complex relationship between kinetic parameters such as K_M , metabolite concentrations and flux within the FBA framework.

As a result, FBA models need additional components to capture the non-linear responses to changes in light and other environmental variables. For example, environment-specific biomass compositions (Poolman *et al.*, 2013, Arnold and Nikoloski, 2014), maximum enzymatic activity (Recht *et al.*, 2014), transcriptomic data (Mintz-Oron *et al.*, 2012, Imam *et al.*, 2015, Scheunmann *et al.*, 2018, Siriwach *et al.*, 2020, Kamsen *et al.*, 2021) and metabolomic data (Kleessen *et al.*, 2015, Sajitz-Hermstein *et al.*, 2016, Pries *et al.*, 2021) have all been used to constrain FBA models in response to changes in light, atmospheric CO₂ concentration, nutrient availability and other environmental variables. While these approaches have been shown to improve the predictive power of constraint-based models, they rely heavily on the availability of context-specific data to model the non-linear metabolic responses.

Dynamic FBA (dFBA) is another approach that can account for the non-linear nature of metabolism. The simplest formalism of dFBA, the static optimization algorithm, involves monitoring concentrations of specific metabolites during an FBA run, and then using ODEs to introduce constraints on appropriate reaction fluxes for the subsequent FBA run (Grafahrend-Belau *et al.*, 2013, Shaw and Cheung, 2018, Schroeder and Saha, 2020). More complicated formalisms of dFBA, dynamic optimization algorithms, trade off the steady-state assumption responsible for maintaining the linear nature of these models for improved representation of the dynamics of metabolic systems. A comprehensive review of dynamic optimization algorithms has been presented in Kleessen and Nikoloski, 2012.

Non-linear processes can be captured explicitly in kinetic modelling which uses mathematical representation of reactions in a metabolic network based on rate equations that account for enzyme kinetics and metabolite concentrations. Kinetic models, such as those composed of ordinary differential equations (ODEs) are capable of simulating not only the steady-state fluxes of the system, but also the dynamic response of reactions to environmental changes. Many kinetic models of leaf metabolism focus on photosynthesis and pathways of related carbon metabolism (Laisk and Walker, 1986, Laisk *et al.*, 1989, Woodrow and Mott, 1993, Sellers *et al.*, 1996, Pearcy *et al.*, 1997, Cox *et al.*, 1999, Fridlyand and Scheibe, 1999, Gombert and Nielsen, 2000, Poolman *et al.*, 2000, Zhu *et al.*, 2007, Miguez *et al.*, 2009, Vos *et al.*, 2010, Zaks *et al.*, 2012, Zhu *et al.*, 2013, McGrath and Long, 2014, Wang *et al.*, 2014, Morales *et al.*, 2018). These range from models describing photosynthesis by two processes (Farquhar *et al.* 1980) to models representing all discrete steps in the process, combined with light activation/de-activation of enzymes (Zhu *et al.*, 2013). The ambition is to extend the metabolic reach of these models, and most recently a model has been assembled that includes glycolysis, gluconeogenesis, the tricarboxylic acid

(TCA) cycle, and chloroplastic nitrogen assimilation, as well as the Calvin cycle, the photorespiration pathway and starch synthesis (Zhao *et al.*, 2021), Kinetic models have been used to analyse the control of both steady-state and transient properties of photosynthesis, and to identify potential targets for photosynthesis and yield improvement. However, it can be difficult to obtain accurate measurements of all the kinetic parameters required for large-scale ODE models; and numerical integration of ODE systems can be challenging due to the different time scales of processes within the model

Hybrid models composed of ODE and FBA models have been proposed as a way of addressing the limitations of both types of modelling, leading to a more accurate modelling framework that remains computationally tractable. Inclusion of kinetic equations based on a power-law formalism associated for key branches of the metabolic network was shown to improve the predictive power of an FBA model of microbial glycolysis (Pozo *et al.*, 2015). The first steps in this direction have also been taken for leaf metabolic models. For example, in a constraint-based model of metabolism across the C3-to-C4 gradient of the maize leaf, sub-models of gas-diffusion and rubisco kinetics were used to compute and constrain the rubisco carboxylase:oxygenase activity ratio in the FBA model (Bogart and Myers, 2016). While Heckmann *et al.*, 2013 used non-linear sub-models to constrain net CO₂ uptake and the fluxes of rubisco carboxylase, rubisco oxygenase, bundle-sheath CO₂ leakage, mesophyll phosphoenolpyruvate carboxylase, bundle-sheath C₄ acid decarboxylation, glycine decarboxylase, exchange of glycine and serine between bundle sheath and mesophyll to constrain fluxes in the C4GEM constraint-based model (Dal'Molin *et al.*, 2010).

Here, we describe a new hybrid leaf model of unprecedented scale, constructed by combining a previously established ODE model of photosynthetic metabolism, the e-photosynthesis ODE model (Zhu *et al.*, 2013), with an FBA model of diel leaf metabolism (Shameer *et al.*, 2019). We explore two ways of integrating the two models: a general loosely coupled approach (LC-ODE-FBA) and a tailored tightly coupled approach (TC-ODE-FBA). We show how the latter approach, while more time-consuming to develop and execute, is capable of capitalizing on the strengths of the individual models while minimizing their weaknesses. Accurate flux predictions of key photosynthetic parameters such as CO₂ assimilation rate, PSII flux and starch accumulation are retained by the coupled model which can make new predictions such as the effect of elevated CO₂ on nocturnal respiration rate that are consistent with measurements of field-grown soybean plants. The broader behaviour of soybean leaf metabolism under three different light intensities, at elevated atmospheric [CO₂], and in growing versus mature source leaves was explored using the TC-ODE-FBA model.

Methods

Plant materials and growth conditions

Mature leaf tissue samples from soybean plants (Glycine max cv. P29A85L) grown at SoyFACE farm County Road 1200 East, Champaign, Illinois (www.igb.illinois.edu/soyface/, 40°02'N, 88°14'W) were collected on August 9, 2019. Four samples were collected from

plants grown in ambient CO₂ (410 ppm) and four from plants grown in elevated CO₂ (550 ppm). Leaf tissue was freeze-dried, powdered, and kept at –80°C until required.

Leaf biomass measurements

Total cell wall and total lipid were analysed by weight following selective extraction according to Poolman et al., 2009. Starch was assayed by enzymatic digestion according to Smith and Zeeman, 2006 except that the tissue was extracted in methanol-chloroform and the released glucose was analyzed by gas chromatography mass spectrometry (GC-MS) according to Lisec et al., 2006. The insoluble material following starch digestion was used for the determination of cell wall sugar composition as follows: the insoluble material was washed twice with 70% (v/v) ethanol and then incubated with 2 M trifluoroacetic acid at 120°C for 1 h to hydrolyse the cell wall to component sugars which were recovered, derivatised and quantified by GC-MS (Lisec et al., 2006). The amino acid content of total protein was determined by selective extraction of total protein, acid hydrolysis and quantification of released amino acids by GC-MS according to Long and Antoniewicz, 2014. The fatty acid content of lipids was analysed by solvent-extraction of total lipid, esterification to produce fatty acid methyl esters (FAMES) and quantification of FAMES by GC-MS according to Laurens et al., 2012. Soluble metabolite profiles were obtained by GC-MS analysis of methanol-chloroform extracts according to Lisec et al., 2006.

The ODE leaf model

The e-photosynthesis model (Zhu *et al.*, 2013) is an ODE-based metabolic model of C₃ photosynthesis encoded in MATLAB. This model was built as a generic C₃ photosynthesis model and was not parameterized for any specific species but built from averages across species where individual kinetic parameters had been determined experimentally. In order to simulate the photosynthetic rate of soybean under various CO₂ conditions, the estimated CO₂ uptake rate of the e-photosynthesis ODE model was calibrated using measured gas exchange data for soybean leaves (Bernacchi *et al.*, 2005). The calibration was achieved by adjusting the maximum enzyme activity of Rubisco ($V_{m_Rubisco}$) in the e-photosynthesis model so that the simulated maximum activity of Rubisco (V_{cmax_s}) was equal to the measured V_{cmax} of soybean (Bernacchi *et al.*, 2005). This required $V_{m_Rubisco}$ to be increased to 1.33 times the value used in the original e-photosynthesis model ($V_{m_Rubisco_o}$) (Fig. S1), Maximum activities of other Calvin-Benson Cycle and starch synthesis enzymes (V_{m_E}) were also linearly transformed so that the simulated maximum RuBP regeneration rate (J_{max_s}) was equal to the measured maximum RuBP regeneration rate (J_{max}) of soybean (Bernacchi *et al.*, 2005). This required V_{m_E} to be increased to 1.36 times the value used in the original e-photosynthesis model ($V_{m_E_o}$) (Fig. S1), Thus, the calibrated maximum rates of the photosynthetic enzyme activities were:

$$V_{m_Rubisco} = V_{m_Rubisco_o} \cdot \alpha_{Rubisco} \quad \text{Equation 1}$$

$$V_{m_E} = V_{m_E_o} \cdot \alpha_E \quad \text{Equation 2}$$

where $\alpha_{Rubisco}$ is 1.33 and α_E is 1.36 (Fig. S1). Adjusted parameters for these enzymes are listed in Table S1. All other parameters were the same as those used in the original e-photosynthesis model (Zhu *et al.*, 2013). Finally, to avoid unreasonable results, constraints

were added to ensure reaction rates of glyceraldehyde-3-phosphate dehydrogenase (GAPDH) and starch degradation were always non-negative.

For each simulation of the kinetic model, the slope of the change of CO₂ assimilation rate with time and each metabolite concentration was checked to evaluate whether the model had reached a steady state.

The FBA leaf model

An updated version (v2.0.0, model curation log presented in Data S2) of the previously published charge and proton-balanced PlantCoreMetabolism model (Shameer *et al.*, 2020) was used in this study to generate FBA models. *Glycine max* specific gene-protein-reaction associations were gathered from the PlantCyc Soy Pathway/Genome Database (PGDB) (<https://www.plantcyc.org/>). Data from the cropPAL database (Hooper *et al.*, 2016) was used to ensure GPR associations were in line with known enzyme subcellular localization. The purpose of mature leaves in higher plants is to use light energy via photosynthesis to generate carbon skeletons and undertake metabolism to load the phloem sap with sugars, amino acids and organic acids for the rest of the plant. Due to the lack of soybean-specific data on petiole phloem sap composition, previously published data from tomatoes (Walker and Ho, 1977, Valle *et al.*, 1998) was used to generate the reaction representing the export of sugars and amino acids into phloem from mature leaves in prescribed proportions (Table S3). As a nodulating legume, allantoin is considered the major leaf nitrogen source (Fujihara *et al.*, 1977). To model this aspect of metabolism, the allantoin catabolism pathway was added to the model from the PlantCyc Soy PGDB. The four hydrolases involved in breaking down allantoin to glyoxylate releasing four moles of NH₄⁺ and two moles of CO₂, were assumed to be ER localized based on annotations of the genes associated on UniProt and findings from Arabidopsis (Takagi *et al.*, 2018). Allantoin uptake into the leaf was assumed to be facilitated via the ENT3 transporter (Niño-González *et al.*, 2019), which has been reported to utilise a proton-symport mechanism (Traub *et al.*, 2007). The charge states of all added metabolites were predicted using MarvinSketch 21.9.0 (<https://www.chemaxon.com>) and all added reactions were charge and proton balanced as previously (Shameer *et al.*, 2018).

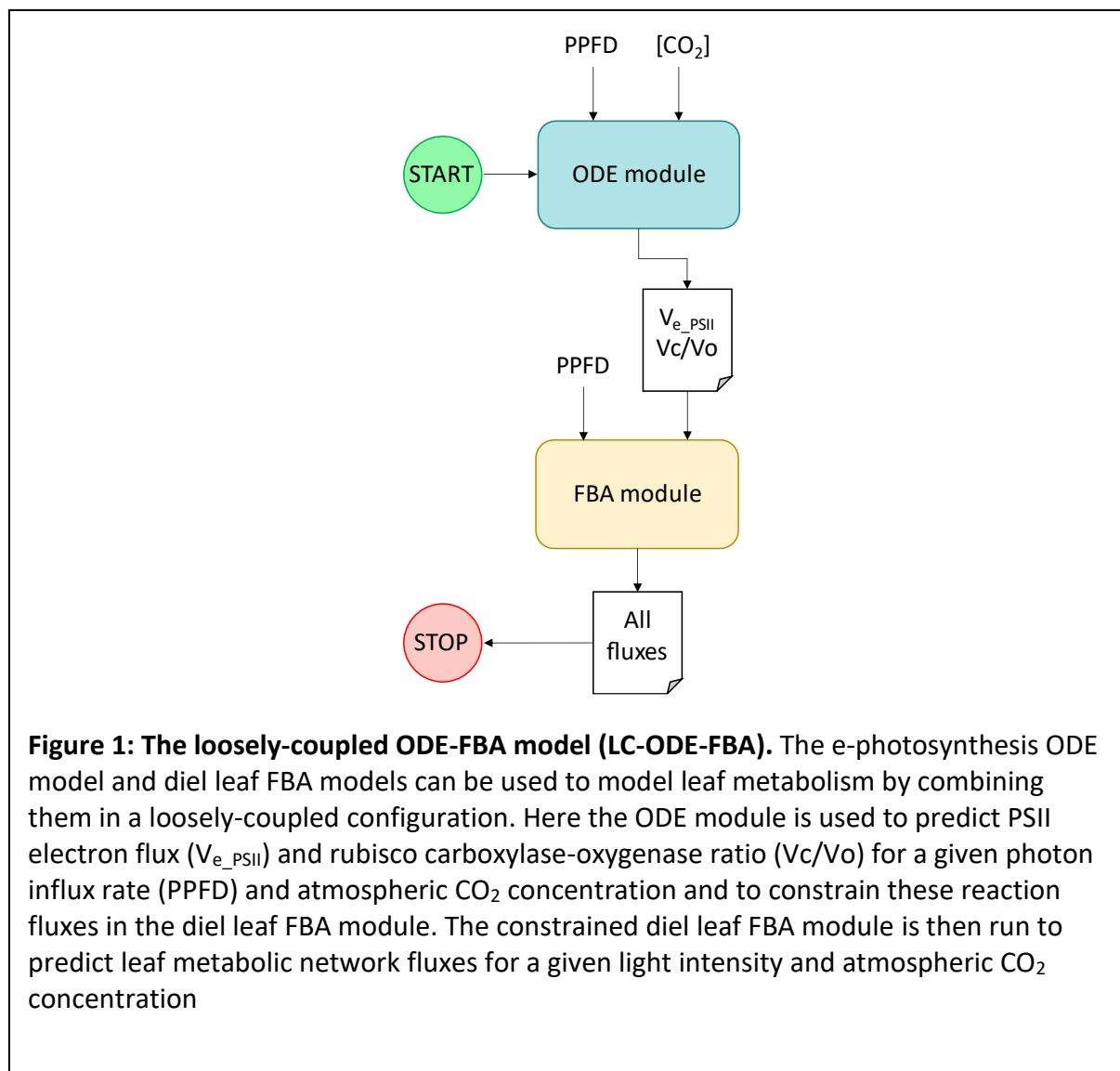
A diel leaf FBA model was generated from the soy-specific version of the PlantCoreMetabolism model using the method described elsewhere (Cheung *et al.*, 2014; Shameer *et al.*, 2019). This entailed duplicating all model elements (compartments, reactions and metabolites) to represent daytime and night-time metabolism and adding 'linker' reactions (reactions that convert daytime metabolites to their respective night-time metabolites and vice versa, to represent diel metabolite accumulation and consumption). Linker reactions were included for chloroplast starch, vacuolar sucrose, vacuolar organic acids and vacuolar amino acids. A complete list of all constraints used to set-up the diel leaf FBA model is presented in Table S4. To model mature leaves, parsimonious FBA (pFBA) was used to model fluxes through the metabolic network maximizing the export of sucrose and amino acids from the leaf.

Loosely coupled ODE-FBA model design

The simplest approach to integrate the e-photosynthesis ODE and the diel leaf FBA model is to use the fluxes predicted by the more mechanistic ODE model to constrain the solution space of the FBA model. This was implemented in a loosely-coupled (LC) ODE-FBA model consisting of two modules, the ODE module (the e-photosynthesis model) and an FBA module. The ODE module was run first and the predicted photosystem II (PSII) electron flux (J_{PSII}) and V_c/V_o flux ratio for a given light intensity and atmospheric $[CO_2]$ were extracted. These values were then used constrain the flux of the corresponding reactions in the diel FBA model (Fig. 1). The ODE and FBA modules were formulated as described in the model execution section and values passed between them using Yggdrasil, a Python package for integrating models with connections between models across languages and scales, while coordinating parallel execution of the models (Lang, 2019).

Tightly coupled ODE-FBA model design

The LC-ODE-FBA model transfers only two of the ODE-predicted fluxes to the FBA module. An alternative approach is to allow the ODE module to predict fluxes through all the chloroplast metabolic reactions, and then to use the FBA model to predict flux through the



chloroplast reactions that were unaccounted for in the ODE model, as well as the reactions in the other subcellular compartments. In this tightly coupled (TC) ODE-FBA model, the additional chloroplast ATP and reducing power costs from the FBA model need to be accounted within the ODE model (Fig. 2).

The ODE module consisted of the soybean e-photosynthesis model, which was modified to account for any additional daytime chloroplast ATP and NADPH costs observed in the FBA module. This was achieved by introducing an additional ATP sink term (v_{ATP_FBA}) to the equation representing the rate of change of chloroplast ATP concentration in the ODE model:

$$d[ATP]_{chl}'/dt = d[ATP]_{chl}/dt - v_{ATP_FBA} \quad \text{Equation 3}$$

Similarly, an NADPH sink term (v_{NADPH_FBA}) was added to the equation representing rate of change of NADPH in the chloroplast to account for the extra NADPH costs:

$$d[NADPH]_{chl}'/dt = d[NADPH]_{chl}/dt - v_{NADPH_FBA} \quad \text{Equation 4}$$

To represent the flow of metabolites between the ODE model and the FBA model, exchange reactions (reactions that represent the import or export of metabolites in the model) for cytosolic TP, cytosolic PGA, cytosolic inorganic phosphate (Pi), cytosolic glycolate, and cytosolic glycerate were added to the FBA model. Exchange reactions for vacuolar malate and vacuolar citrate were also added to the FBA model to enable it to represent organic acids accumulation and remobilization fluxes. To allow the ODE model to supply ATP and NADPH to the FBA chloroplast, reactions for chloroplast ATP and NADPH generation from ADP and NADP⁺ respectively, were added to the FBA model.

The TC-ODE-FBA formulation does not use a diel FBA model, because the ODE model only accounts for chloroplast metabolism in the light. This means that the FBA model needed to be constrained to force it to accumulate malate and remobilise citrate during the day. From separate diel FBA leaf model predictions, the following relationships between starch accumulation and organic acid accumulation /remobilization were noted (Supplemental Table 7):

$$V_{MAL_acc} = 0.71 \times V_{STARCH_acc} \quad \text{Equation 5}$$

$$V_{CIT_acc} = -0.56 \times V_{STARCH_acc} \quad \text{Equation 6}$$

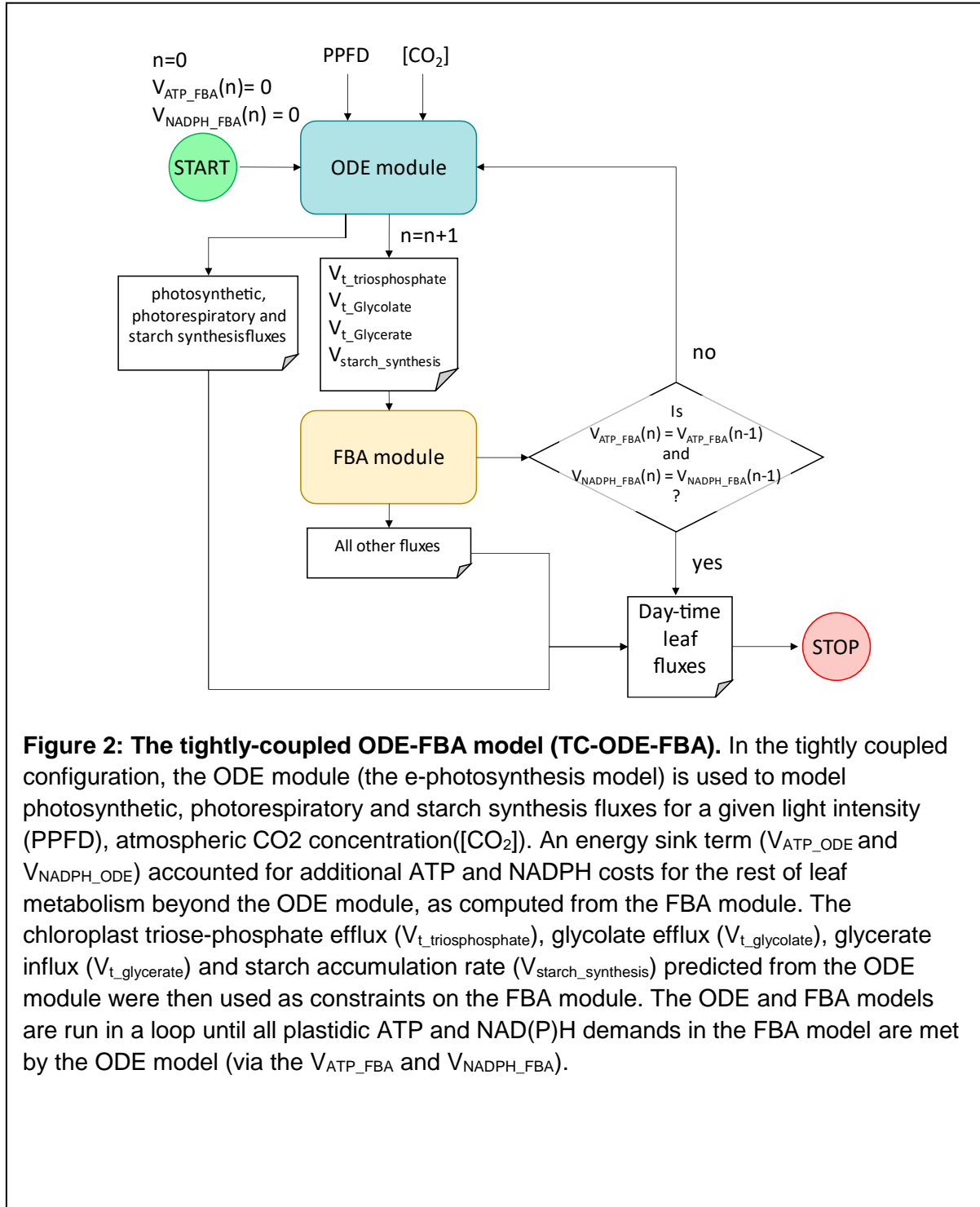
where V_{MAL_acc} , V_{CIT_acc} and V_{STARCH_acc} are malate, citrate and starch accumulation fluxes for which positive values suggest accumulation and negative values suggest remobilization of accumulated metabolites. These equations were used to constrain the respective fluxes in the FBA model.

To run the TC-ODE-FBA model, the initial values for v_{ATP_FBA} and v_{NADPH_FBA} were set to 0, and the steady-state values predicted by the ODE module for chloroplast triose-phosphate (TP) and 3-phosphoglycerate (PGA) export and starch accumulation rate were recorded. In the FBA module, the exchange reactions for TP and PGA were constrained to the values recorded in the ODE module. Likewise, the values for the chloroplast glycolate efflux and

glycerate influx predicted by the ODE module were used to constrain the equivalent exchange fluxes in the FBA model. The rate of starch accumulation in the ODE model was also used to constrain malate accumulation and citrate remobilization rates in the vacuole of the FBA model based on equations 5 and 6, respectively. Fluxes through reactions generating ATP and NADPH in the FBA model were constrained based on v_{ATP_FBA} and v_{NADPH_FBA} fluxes from the ODE module. pFBA was then used to predict a flux distribution in the FBA model that maximised the export of sucrose and amino acids from the leaf to the phloem. A feasible solution was guaranteed because there were no obligatory demands on the FBA model other than the non-growth associated maintenance (NGAM), which was constrained as a function of light intensity (Töpfer *et al.*, 2020), and hence the ODE steady-state solution for the same light intensity should fall within FBA solution space.

The fluxes through the ATP and NAD(P)H shuttles (plastid nucleotide transporter NTT and malate dehydrogenase activity respectively) to the chloroplast in the FBA module were observed to check whether the chloroplastidic ATP and NADPH demands in the FBA model were met by the ODE model. Since FVA analysis revealed that ATP shuttling via NTT and PEP-pyruvate shuttle contributed equally to the optimization problem, the flux weighting on the NTT reaction was changed from 1 to 0.5 during the minimization of sum of fluxes stage of pFBA to ensure that all the ATP was shuttled via the NTT reaction during pFBA. If the shuttles were found to be actively importing ATP or NAD(P)H into the FBA chloroplasts, then the values of v_{ATP_FBA} and v_{NADPH_FBA} were updated to account for the ATP and NADPH shuttled; and the ODE and FBA modules were run again. Only when the net ATP and NADPH demand in the FBA chloroplast were found to met by v_{ATP_FBA} and v_{NADPH_FBA} (i.e. ATP and NADPH shuttles carried fluxes less than 0.005), were the ODE and FBA (representing daytime metabolism) models deemed to have reached a consensus. The loop was then broken and fluxes for daytime metabolism from both modules were recorded.

Night-time leaf metabolism in the TC-ODE-FBA set-up was modelled using another copy of the soy-specific PlantCoreMetabolism FBA model. This model was set up by setting photon uptake to 0 and constraining starch degradation, malate remobilization and citrate accumulation rates based on total starch accumulated during the photoperiod, such that at dawn all the accumulated starch was depleted. Again, pFBA was used to model fluxes maximizing the night-time export of sucrose and amino acids from the leaf to the phloem. As with the LC-ODE-FBA model, ODE and FBA modules were formulated as described in the model execution section and put together for the TC model using the yggdrasil framework (Lang, 2019).



Modelling metabolism of mature soybean leaves across a range of light intensities and atmospheric CO₂ concentrations

The two original models (ODE leaf model, the diel FBA leaf model) and the two hybrid models (LC-ODE-FBA and TC-ODE-FBA) were used to model the assimilation rate (A) in leaves experiencing a range of light intensities and atmospheric CO₂ concentrations (C_a). The resulting assimilation rates were used to generate $A-C_i$ and A -PPFD curves for each model, based on the assumption that $C_i = 0.7 \times C_a$, where C_i is the intercellular [CO₂]. Previously published data on assimilation rates observed under different intercellular [CO₂] and saturating light intensities (Morgan *et al.*, 2004, Sun *et al.*, 2014) and assimilation rates observed under different light intensities and ambient [CO₂] (Zhang *et al.*, 2011, Yao *et al.*, 2017, Haile *et al.*, 2003) were used to evaluate the accuracy of the model predictions.

Modelling metabolism of mature soybean leaves from plants grown in free air CO₂ enrichment (FACE) experiments

Records of diurnal variations of canopy incident light intensity for soybean in ambient [CO₂] and [CO₂] elevated to 550 $\mu\text{mol mol}^{-1}$ under open air conditions using FACE technology over the growing season (Rogers *et al.*, 2004) were collected. Hourly light-intensities during the experiment were estimated by linear interpolation. Daytime leaf metabolism for each hour of the photoperiod was modelled using the ODE, FBA, LC-ODE-FBA and TC-ODE-FBA set-ups, and CO₂ assimilation, PSII electron flux and starch accumulation rates were recorded. Leaf starch content at noon predicted by each model was calculated by adding up all hourly starch accumulation rate predictions from dawn to noon. Night-time metabolism in the TC-ODE-FBA model driven by total starch accumulated during the photoperiod, accounting for changes in day-length over the growing season, was modelled using an FBA model as described earlier.

Modelling metabolism in mature and growing soybean leaves

The TC-ODE-FBA model was used to compare metabolism of mature and growing soybean leaves at 400 $\mu\text{mol mol}^{-1}$ atmospheric [CO₂] and 1000 $\mu\text{mol m}^{-2}\text{s}^{-1}$ PPFD. Mature leaves were modelled using TC-ODE-FBA with an objective function to maximize the export of sucrose and amino acids into the phloem using pFBA. In order to model growing leaves, the biomass composition of soy leaf was experimentally determined (Supplemental Table S2) and a biomass reaction representing the accumulation of biomass elements in the observed ratios was added to the FBA model. The growing leaf was then modelled by optimizing the flux distribution to maximize flux through the biomass reaction using pFBA during the FBA runs of TC-ODE-FBA model.

Model execution

The ODE model was executed on MATLAB 2020a using its ODE15s solver. All FBA models were run on python 3.7.6 using the cobrapy v0.17.1 package and the default GLPK solver. Yggdrasil was used to coordinate the execution of the two models in their native environments and the transfer of information between them. All models, MATLAB scripts, python scripts, yggdrasil YAML files and input files required to run the FBA model, ODE

model, LC and TC models are available in the github repository:

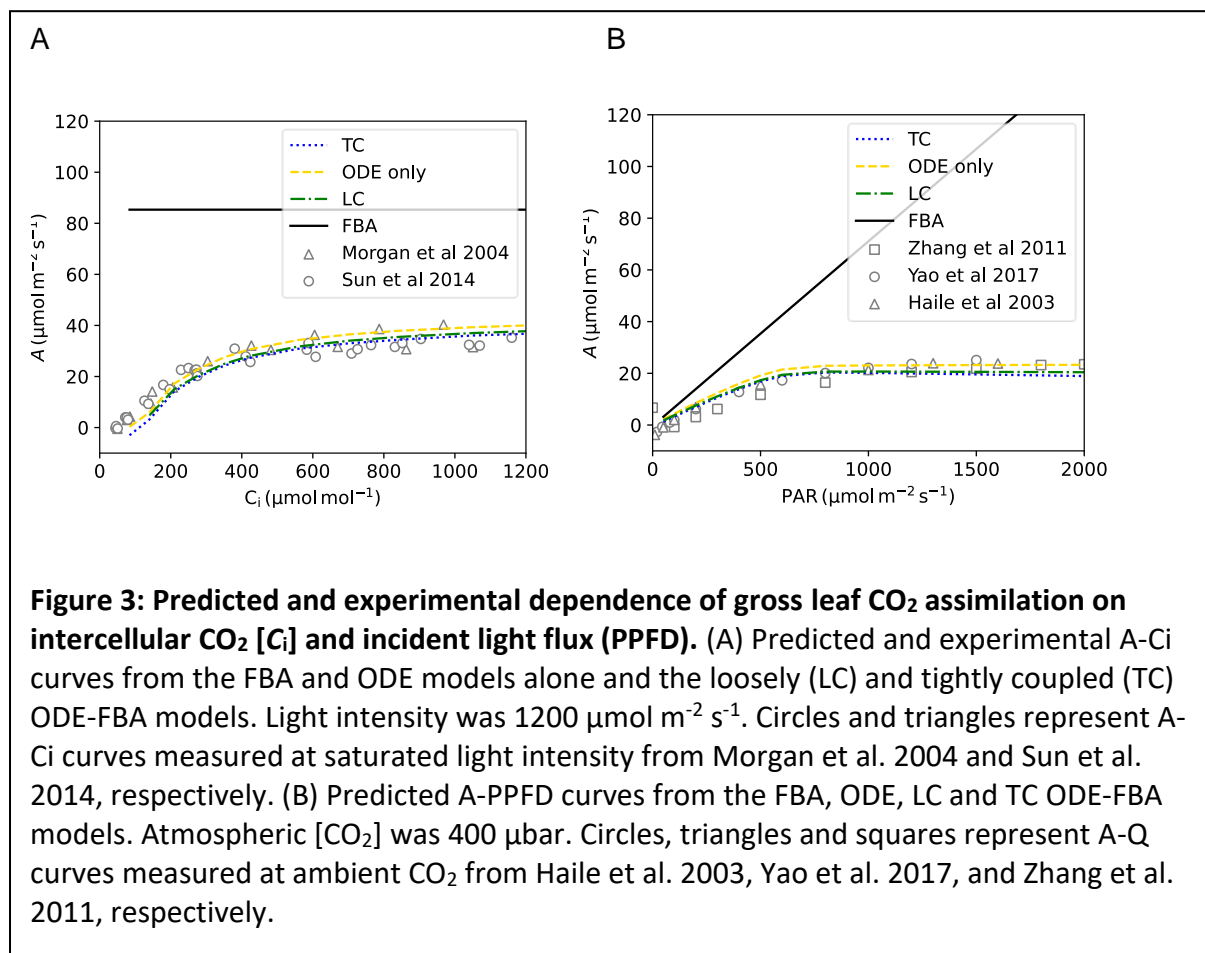
https://github.com/cropsinsilico/ODE_FBA_Photosynthesis2021

Results

Coupled-ODE-FBA models make accurate predictions of the effect of light intensity and atmospheric [CO₂] on photosynthetic assimilation rate

The e-photosynthesis ODE model accurately accounts for the effect of atmospheric [CO₂] and light intensity, with the model-predicted rate of photosynthetic carbon assimilation closely matching experimentally measured values (Fig 3A, B). In contrast, the FBA model fails to reflect changes in atmospheric [CO₂] and light intensity: the predicted photosynthetic assimilation rate is insensitive to [CO₂] (Fig 3A) and the model predicts a linear response to light intensity (Fig 3B). Figure 3 also shows that the ODE, LC-ODE-FBA and TC-ODE-FBA models predicted very similar *A* values to each other across a range of light intensities and atmospheric [CO₂] with the coupled models predicting *A* values slightly lower than the ODE model, although still close to experimental values. Because the PSII electron flux is constrained to the corresponding flux in the ODE model, both ODE and LC-ODE-FBA models carry the same flux through their respective photosynthetic linear electron flow (LEF) pathways, generating the same amount of reducing power for a given light intensity. The LC-ODE-FBA model however has additional reducing power demands when compared to the ODE model (maintenance and photorespiratory N-refixation), so it predicts lower *A* values. The TC-ODE-FBA model also predicts slightly lower *A* values compared to the ODE model because of the higher ATP and reducing power demand due to accounting for maintenance, photorespiratory N-refixation and sucrose biosynthesis (see Table S4 and S5). Maintenance costs (defined in the FBA component) were observed to decrease TC-ODE-FBA assimilation rate by 11% in saturating light conditions. Predicted *A* values from both coupled models fell within the range of *A* values reported in previously published experiments (Fig 3A and 3B).

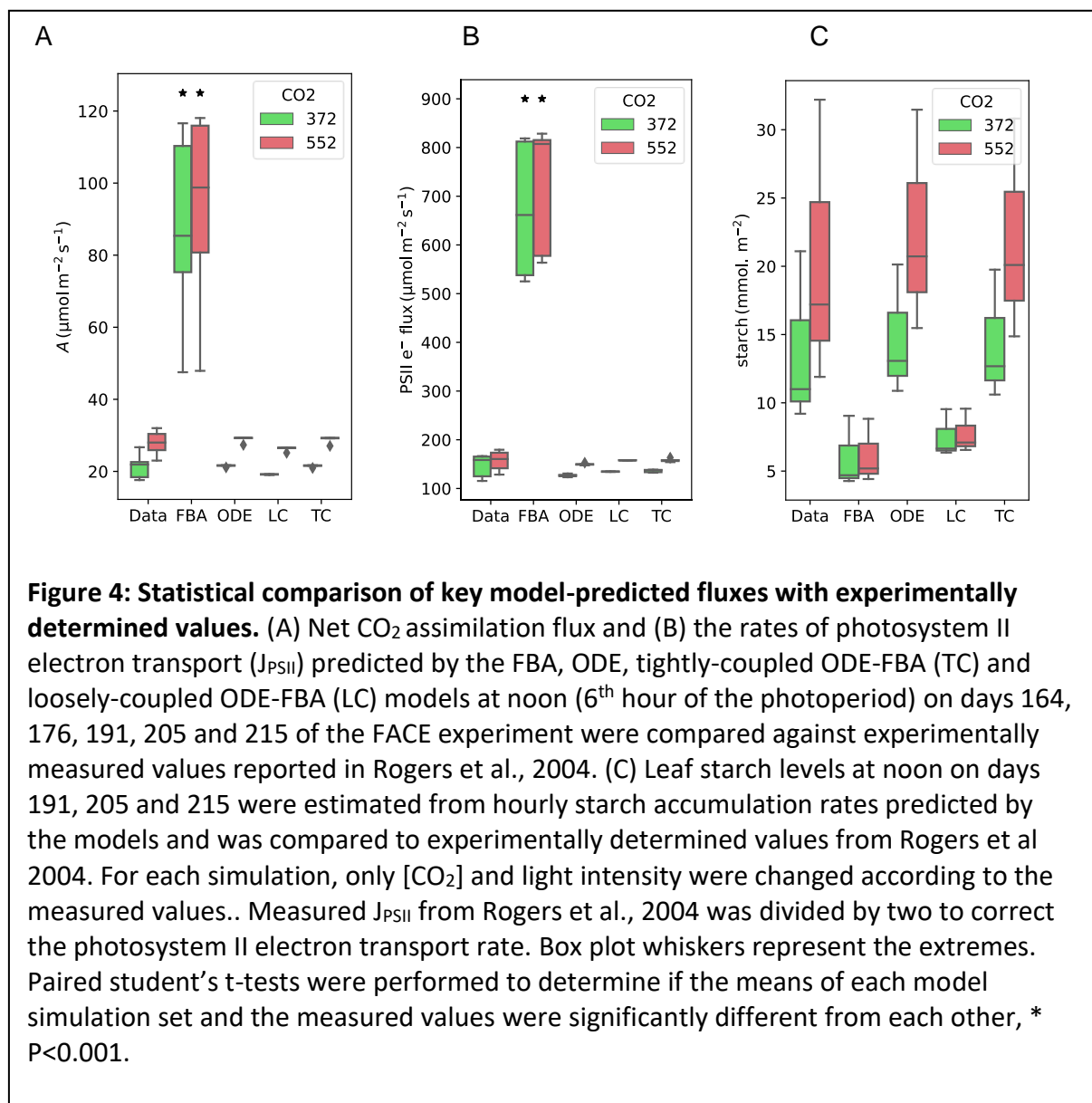
While both coupled models predicted very similar A values, there is a major difference in the energetic flexibility of the two models. In the LC-ODE-FBA model, LEF (handled by the FBA module) is limited by the PSII electron flux predicted by the ODE module, but the model is free to run unconstrained cyclic electron flow (CEF) to generate additional ATP to meet its energy demands (as is evident from the 'Ferredoxin_Plastoquinone_Reductase_p1' flux in Supplemental Data S2). In contrast, in the TC-ODE-FBA model the relative rates of LEF and CEF are dictated by the kinetic parameters of the relevant photosynthetic electron transport chain complexes and this results in a more limited ATP supply from photons. Hence the TC-ODE-FBA model predicted utilisation of the TCA cycle and mitochondrial ATP synthesis to meet the remainder of its ATP demand. For example, when modelling metabolism in leaves grown in a $1000 \mu\text{mol m}^{-2} \text{s}^{-1}$ light intensity and 400 ppm $[\text{CO}_2]$, the LC-ODE-FBA model gave a CEF-LEF ratio of 0.45 compared to a value of 0.33 in TC-ODE-FBA model. On the other hand, the LC-ODE-FBA model did not predict any mitochondrial ATP synthesis compared to a value of $7.24 \mu\text{mol ATP m}^{-2} \text{s}^{-1}$ in the TC-ODE-FBA model. The LC-ODE-FBA and TC-ODE-FBA models also showed significant difference with regards to run-times.



While the LC-ODE-FBA model only needed to run its ODE and FBA components once, the TC-ODE-FBA model needs to run until both its ODE and FBA components achieved “convergence” which was noted to happen within 4-10 cycles, resulting in the TC-ODE-FBA model taking 4 to 10 times longer to run than the LC-ODE-FBA model (Supplemental Fig S3). A summary of the different capabilities of the ODE, FBA, LC-ODE-FBA and TC-ODE-FBA models is presented in Supplemental Table S8.

Comparing predicted rates of photosynthesis and starch synthesis with measured data

The predictive accuracy of the coupled ODE-FBA models was assessed by comparing the predicted rates of CO₂ assimilation, PSII electron transport flux and starch accumulation in the FBA, ODE, LC-ODE-FBA and TC-ODE-FBA models with experimental data from soybean grown in FACE experiments (Rogers et al., 2004). The predicted fluxes from each model are listed in Supplemental Data S2-5. The FBA model substantially overestimated *A*, while the ODE model, LC-ODE-FBA and TC-ODE-FBA models predicted accurate values for *A* at two different atmospheric CO₂ concentrations (no statistically significant difference to the experimentally measured data) (Fig. 4A). Similarly, all the models except the FBA model, accurately predicted *J*_{PSII} in both ambient and elevated [CO₂] (Fig. 4B). Elevated [CO₂] resulted in a higher *J*_{PSII} than ambient [CO₂], but the proportional increase was much less than for *A* (Fig 4B). Turning to daytime starch accumulation, both the FBA and LC-ODE-FBA models underestimated leaf starch levels at noon to a statistically significant degree (Fig.



4C). In contrast the ODE and TC-ODE-FBA models predicted statistically accurate noon starch levels in both ambient and elevated [CO₂] (Fig. 4C).

The improved prediction accuracy for starch accumulation by the TC-ODE-FBA model can be attributed to the fact that it utilises the ODE module to predict starch accumulation rates by accounting for the kinetics of photoassimilate partitioning. The LC-ODE-FBA model, on the other hand, relies on the FBA component to predict the starch accumulation rate, which is significantly influenced by model parameters such as maintenance costs and the day-night phloem export rate ratio. However, these parameters were not based on soy data and so the predicted starch accumulation rate is less likely to be accurate.

A parameter sensitivity analysis was undertaken to test the robustness of the predictive accuracy of the TC-ODE-FBA model to the various parameter choices and assumptions contained within the model (Supplemental Information S1, Supplemental Table S9). Key assumptions and parameters in the FBA module, such as the maintenance cost, the constraint on the ratio of starch to carboxylic acid accumulation, and the constraint on phloem metabolite composition, had negligible effects on the accuracy with which the TC-ODE-FBA model predicted *A* and starch accumulation at both ambient and elevated [CO₂]. In contrast, varying 11 out of the 309 kinetic parameters by $\pm 50\%$ was noted to impact the TC-ODE-FBA model CO₂ assimilation rate predictions (and hence the ability of the model to predict leaf starch content as well). A further five kinetic parameters were observed to significantly influence starch accumulation rate predictions. While overall, this does suggest that the model is robust to small variations in the parameters used, it does highlight, perhaps unsurprisingly, sensitivity to a relatively small number of the kinetic parameters. Future work could look to determining more accurate values for these specific parameters and checking that they do not change in soybean plants grown under different environments.

The tightly coupled ODE-FBA model predicts a higher night-time respiration rate in soybean grown under elevated [CO₂]

The TC-ODE-FBA model can be used to model night-time leaf metabolism using the outputs from the daytime model and a single-phase nocturnal FBA module. The FBA module predicted that the oxidative pentose phosphate pathway (PPP) and pyruvate dehydrogenase (PDH) were responsible for a significant fraction of night-time CO₂ evolution, with only a small fraction of total CO₂ evolved originating from the TCA cycle. This was found to be a consequence of the organic acid accumulation/remobilization constraints in the model (equation 5 and 6). Malate remobilized from the vacuole was oxidized to oxaloacetate (OAA) via malate dehydrogenase, contributing to a significant fraction of the TCA flux. A small fraction of this malate was also used to generate pyruvate via malic enzyme. A significant fraction of the citrate generated in the TCA cycle was observed to accumulate in the vacuole to comply with the citrate accumulation constraints. As a result of this, considerably smaller flux was observed in the remainder of the TCA cycle (citrate to malate).

The TC-ODE-FBA model was used to predict the effect of the atmospheric [CO₂] on respiratory CO₂ production in soybean leaves, using parameters from a soybean FACE experiment. The TC-ODE-FBA model predicted a higher respiration rate under elevated CO₂ (Fig. 5) consistent with what has been observed experimentally (Rogers *et al.*, 2004). A parameter sensitivity analysis (Supplemental Information S1; Supplemental Table S9)

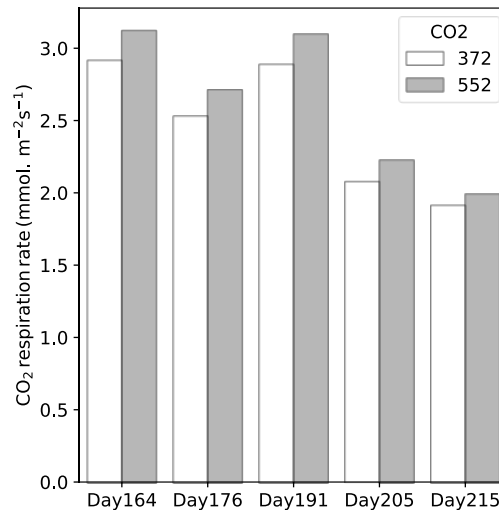


Figure 5: The tightly coupled ODE-FBA model predicts a higher night-time respiration rate in elevated [CO₂]. The tightly coupled ODE-FBA model was used to model night-time metabolism under ambient and high [CO₂] FACE conditions (days 164, 176, 191, 205 and 215) and the CO₂ respiration rate computed from.... [Sanu, please explain what you did: was it just the CO₂_tx rxn or did you sum all CO₂-generating fluxes?

Table 1: Night-time CO₂ producing and consuming processes in leaves modelled under Day 164 FACE conditions

Metabolic process	CO ₂ flux (μmol m ⁻² s ⁻¹)	
	[CO ₂] = 372 ppm	[CO ₂] = 552 ppm
Pentose phosphate pathway	1.28	1.10
Pyruvate dehydrogenase	1.09	1.54
TCA cycle	0.27	0.05
Malic enzyme	0.22	0.33
Allantoin degradation	0.03	0.06
Amino acid biosynthesis	0.01	0.02
CO ₂ respiration	-2.91	-3.12

showed that in all cases where a model solution was achieved, a higher respiration rate was observed under elevated CO₂ if the same parameter value was used at both CO₂ levels.. Table 1 lists fluxes through all the metabolic processes involved in the production and consumption of CO₂ in leaves at night on Day 164 of the FACE experiment as modelled by the TC model. Here we see a higher PDH and malic enzyme flux in elevated [CO₂] compared to the ambient conditions. The model proposes this because of the increased availability of vacuolar malate in elevated [CO₂] (a consequence of equation 5 and increased day-time starch accumulation rate predicted by the ODE module, Fig 4C). With increased reducing power being generated by PDH and malic enzyme, the OPPP flux was observed to

drop in elevated [CO₂] conditions. and there was also a predicted decrease in the TCA cycle flux from citrate to malate. The latter also reflected the increased citrate accumulation flux (a consequence of equation 6 and increased day-time starch accumulation rate predicted by the ODE module, Fig. 4C). Overall, a higher respiration rate at elevated CO₂ was observed through increased night-time leaf metabolic activity, which was a consequence of the higher transitory starch store predicted by the ODE component of the hybrid model in elevated CO₂ conditions.

Metabolism under different light intensity and [CO₂] conditions

The TC-ODE-FBA model was used to model the effect of light intensity on daytime metabolism in ambient [CO₂] under low (LL), medium (ML) and saturating light (HL) conditions (300, 600 and 1000 $\mu\text{mol photons m}^{-2} \text{s}^{-1}$, respectively). Major fluxes (those above a threshold of 0.3 $\mu\text{mol.m}^{-2}\text{s}^{-1}$) predicted at LL, ML and HL are depicted in Figs. 6A, 6B and 6C, respectively. Among the many differences, the dissipation of excess light energy, which was primarily via non-photochemical quenching (NPQ), and the fluxes associated with starch accumulation were found to increase with increasing light intensity. The model also predicted sucrose export rates of 0.72, 1.11 and 0.95 $\mu\text{mol m}^{-2} \text{s}^{-1}$ for the LL, ML and HL conditions, respectively. This pattern was the result of an increased allocation of C towards starch in HL (22% and 39.3% of net assimilated C in ML and HL respectively). The model also predicted a rubisco Vc/Vo ratio of 2.96 for all three light conditions, and hence photorespiration and the associated N refixation fluxes were observed to follow the CO₂ assimilation rate pattern observed in Fig 3B. Since NGAM in the model is a function of the incident light intensity, a higher mitochondrial ATP synthase flux (generating ATP to meet NGAM demand) was observed at higher light intensities.

The TC-ODE-FBA model was also used to study the effect of elevated [CO₂] on leaf metabolism by modelling metabolism in 800 ppm [CO₂] and 1000 $\mu\text{mol photon m}^{-2} \text{s}^{-1}$ light intensity (HL-E; Fig 6D). Compared to HL, HL-E showed decreased photorespiration and an increased Calvin cycle flux resulting in higher chloroplastic ATP and NADPH consumption. As a result, more of the incident light was used for photochemistry to meet this higher energy demand and a lower NPQ was predicted. The reduced photorespiratory rate at elevated CO₂ also resulted in a reduced ammonia reassimilation flux and the associated energy demand. The HL-E model also predicted a higher starch accumulation rate in agreement with experimental observations (discussed earlier), and since daytime vacuolar malate accumulation and citrate remobilization fluxes in the model were constrained to the starch accumulation rate, the HL-E prediction showed an increased contribution of night-time citrate to the TCA cycle, permitting the model to divert more phosphoenolpyruvate towards malate biosynthesis via anaplerotic C fixation. This reduced the predicted pyruvate dehydrogenase flux in HL-E compared to HL. The complete set of flux predictions for LL, ML, HL and HL-E conditions is provided in Supplemental Data S6.

Metabolism in mature and growing leaves

The predictive power of the TC-ODE-FBA model was explored further by comparing the metabolism of fully-expanded mature leaves and growing leaves grown at 1000 $\mu\text{mol.m}^{-2}.\text{s}^{-1}$

PPFD and 400 ppm CO₂. A complete list of the predicted reaction and transport fluxes in mature and growing leaves is given in Supplemental Data S7. In total, fluxes were predicted for 728 metabolic reactions and transport steps in mature leaves and 837 in growing leaves. A simplified representation of the major fluxes in mature and growing leaves during the day and night is shown in Fig. 7. A comparison between the predicted flux distributions for the two leaf types shows that the dominant daytime fluxes were photosynthetic electron transport and ATP synthesis, the Calvin cycle and photorespiration. These fluxes were essentially identical in the two leaf types, as would be expected given that these photosynthetic fluxes are primarily determined by the invariant light flux and atmospheric CO₂ concentration. Other fluxes in the wider metabolic network also showed some similarities, most notably a non-cyclic TCA flux, which is consistent with ¹³C labelling results (Xu *et al.*, 2021).

However, there were also notable differences in the predicted flux distributions between the two leaf types. Mature leaves used assimilated carbon to export sugars and amino acids to the phloem while growing leaves used assimilated carbon to meet the requirement for synthesis of new biomass components (Fig. 7). As a result, during the day, there were higher rates of N uptake, amino acid biosynthesis and anaplerotic C-fixation in the growing leaf model to meet the protein demand for growth. The growing leaf model also predicted higher rates of mitochondrial ATP synthesis, primarily to support additional protein synthesis (Figs 7A and 7B). This is also evident from the ATP budgets calculated from the predicted flux distributions in the mature and growing leaf models (Table 2). In the growing leaf model, fluxes were also observed in reactions associated with the biosynthesis of cellulose, xylan, phosphatidate, palmitoyl acyl carrier protein (ACP), palmitoleoyl ACP, stearoyl ACP, oleoyl ACP, octadecadienoyl ACP, arachidoyl ACP, eicosenoyl ACP and behenoyl ACP. These fluxes were relatively small and are not depicted in Fig 7B. In contrast the mature leaf model did not show any flux through these pathways.

Differences between the two leaf types were also apparent in the predicted flux distributions for nocturnal metabolism (Figs 7C and 7D). The mature leaf model used carbon and energy generated from starch degradation to generate sucrose and amino acids while the growing leaf model used the same to generate protein, lipids and cell wall (fluxes representing lipid and cell wall biosynthesis and parts of the regular TCA cycle are not depicted in Figs 7C and 7D since these fluxes were relatively very small). The growing leaf model also showed higher nocturnal N uptake, amino acid biosynthesis and anaplerotic C-fixation similar to daytime metabolism. In the case of the growing leaf model, higher nocturnal fluxes were also apparent in glycolysis, the TCA cycle and the mitochondrial electron transport chain (mETC) (Fig. 7D) to support the energy demand involved in the synthesis of biomass components.

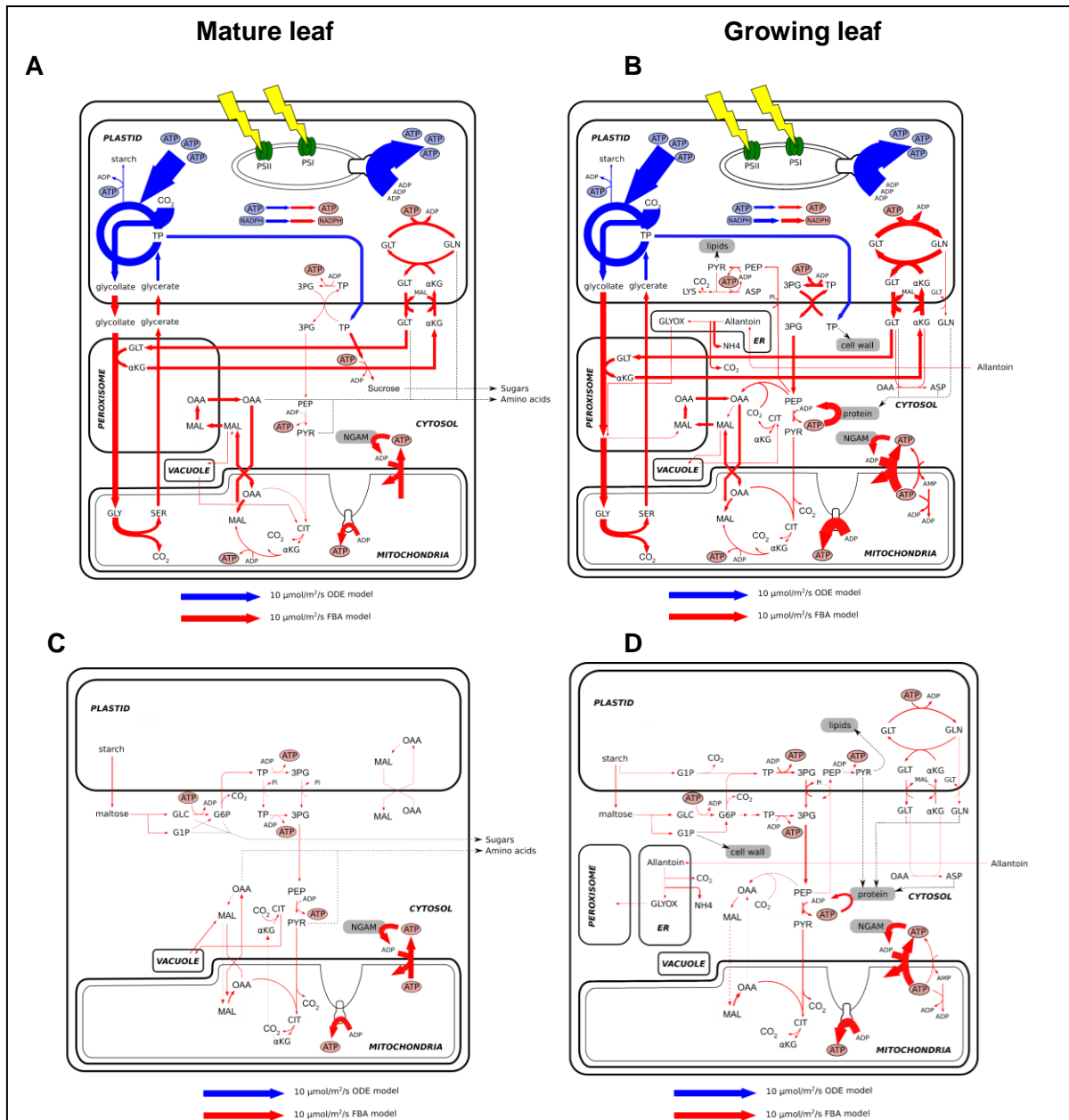


Figure 7: The tightly-coupled ODE-FBA model can be used to predict metabolic network fluxes in mature and growing leaves in the light and the dark. The tightly coupled ODE FBA model was used to model mature and growing leaves under PPFD $1000 \mu\text{mol m}^{-2}\text{s}^{-1}$ and $[\text{CO}_2]$ of 400 ppm. In the TC configuration, the ODE model predicts chloroplast metabolism (fluxes in blue) and provides precursors for the FBA model to model fluxes in other compartments and chloroplast metabolic pathways outside the scope of the ODE model (fluxes in red). The FBA model was configured to model mature leaves exporting sucrose to the phloem during the day (A) and night (C) or growing leaves synthesizing and accumulating biomass during the day (B) and night (D). For clarity only fluxes above a threshold of $0.3 \mu\text{mol} \cdot \text{m}^{-2} \cdot \text{s}^{-1}$ are depicted. Arrow thicknesses are proportional to flux values. NGAM, Non-growth associated maintenance. Abbreviations: 3PG, 3-phosphoglycerate; ASP, aspartate; CIT, citrate; G1P, glucose 1-phosphate; G6P, glucose 6-phosphate; GLC, glucose; GLN, glutamine; GLT, glutamate; GLY, glycine; LYS, lysine; MAL, malate; OAA, oxaloacetate; PEP, phosphoenolpyruvate; Pi, inorganic phosphate; PYR, pyruvate; SER, serine; TP, glyceraldehyde 3-phosphate; αKG , 2-oxoglutarate; GLYOX, glyoxylate.

Table 2: ATP production and consumption in the tightly coupled ODE-FBA model during the day. Leaf metabolic fluxes for PPFD = 1000 $\mu\text{mol}/\text{m}^2/\text{s}$ and $[\text{CO}_2]$ = 400 ppm were predicted by the tightly-coupled ODE-FBA model. Reaction fluxes involving the consumption and production of ATP from both model components, represented by negative and positive ATP flux values respectively, were used to tabulate ATP consumption and production.

Metabolic process	ATP flux ($\mu\text{mol m}^{-2}\text{s}^{-1}$)	
	Mature	Growing
Chloroplast ATP synthesis	116.50	116.61
Mitochondrial ATP synthesis	7.24	17.91
Glycolysis	1.19	7.28
SuccinylCoA synthase	1.12	1.22
Structural carbohydrate	0.00	-0.13
Amino acid biosynthesis	-0.04	-1.32
Sucrose synthesis	-1.04	0.00
Starch biosynthesis	-1.33	-1.33
Photorespiration	-4.67	-4.67
GS-GOGAT	-4.83	-8.51
Maintenance	-7.69	-7.69
Protein biosynthesis	0	-12.86
Calvin Benson cycle	-106.42	-106.43

Discussion

Tight coupling provides a better hybrid ODE-FBA model

The LC-ODE-FBA configuration is the simplest way to integrate ODE and FBA leaf models and it is similar to the individual FBA runs in previous dFBA models (Grafahrend-Belau *et al.*, 2013, Shaw and Cheung, 2018). In this set-up both model elements need to be run only once and hence computation is fast and can be run independently on different platforms with only minimal information being passed from the ODE model to the FBA model. Additionally, the FBA component of the LC-ODE-FBA configuration is a diel leaf FBA model and hence this configuration inherits all the advantages of diel leaf FBA models, such as the ability to predict day-night amino acid and organic acid accumulation rates (Cheung *et al.*, 2014). While it has its advantages, the LC-ODE-FBA model also has a major limitation. Kinetic equations based on metabolite and enzyme concentration and reaction kinetics determine the fate of photoassimilates in the ODE model. This part of the ODE model is ignored in the LC-ODE-FBA model, and so while the assimilation rate was predicted accurately, photoassimilate partitioning prediction was inaccurate (Fig 4).

In contrast, the TC-ODE-FBA model accurately predicted both assimilation rate and photoassimilate partitioning. It achieves this by using the ODE model to predict chloroplastidic fluxes and then using the FBA model to predict fluxes outside the scope of the ODE model, while allowing the FBA model to relay its chloroplastidic energy demand back to the ODE model via the v_{ATP_FBA} and v_{NADPH_FBA} fluxes. These fluxes are fed into the ODE model as steady-state ATP and NADPH sinks, respectively, since they represent the demands of the steady-state FBA model. Under all scenarios modelled here, the ODE model was able to accommodate the constant v_{ATP_FBA} and v_{NADPH_FBA} sinks. However, very large v_{ATP_FBA} and v_{NADPH_FBA} sink fluxes could potentially prevent the ODE model from achieving a feasible solution (by quickly bringing the NADPH or ATP concentration to below zero). The likelihood of this was observed to be higher in energy-limited scenarios such as extremely low light, or low-light at elevated $[CO_2]$ condition. One possible workaround for this issue is to gradually increase the v_{ATP_FBA} and v_{NADPH_FBA} sink fluxes from 0 to its actual value once the model has been able to achieve a temporary steady state. It should be noted that under extreme energy-limited conditions, the e-photosynthesis model is unable to achieve steady state even in isolation (equivalent to v_{ATP_FBA} and v_{NADPH_FBA} fluxes set to 0). More work on the ODE model is required to overcome this issue. Nevertheless, with this configuration, the TC-ODE-FBA model was able to model leaf metabolism for all conditions discussed in this study, and the results show that the ODE and FBA components complemented each other, thus overcoming many of their individual limitations.

Although both modules needed to be run multiple times in a loop on the same platform, the TC-ODE-FBA model offers a much higher predictive power compared to the LC-ODE-FBA model. In addition, parameter sensitivity analysis showed that the principal predictions (i.e. higher assimilation, starch accumulation and night-time respiration rates at higher $[CO_2]$) held true for $\pm 50\%$ variation in any modelling parameter, as long as a steady-state was achievable. It should however be noted that the parameter values were assumed to be the same in both ambient and elevated CO_2 conditions here, which may be the case for many kinetic parameters, but non-kinetic parameters such as NGAM costs and organic acid – starch accumulation / remobilization rate ratios are likely to be different under different environmental conditions.

Another significant advantage of TC-ODE-FBA over LC-ODE-FBA is its ability to model the dissipation of excess light energy. The TC-ODE-FBA analysis of low-light (LL), medium-light (ML) and saturating-light (HL) conditions showed that energy dissipation increased with light intensity (Fig. 6A, B and C), in agreement with previous observations (Rahimzadeh-Bajgiran *et al.*, 2017, Nicol *et al.*, 2019). The model also predicted a decrease in NPQ in leaves under saturating light when atmospheric $[CO_2]$ increased (Figs 6C and D), which has also been previously established in tobacco (Miyake *et al.*, 2005, Dahal *et al.*, 2018). While the model can make many qualitative predictions about the dissipation of excess energy, it still has limitations. Since AOX falls under the FBA component, its ability to dissipate excess energy is not considered in the current TC-ODE-FBA set up. As a result, the model is unable to explore the role of AOX in the light-stress response (Dahal *et al.*, 2018). The model is also unable to depict the sensitivity of V_c/V_o ratio to incident light. For example, TC-ODE-FBA model predicted a constant V_c/V_o ratio of 2.96 for LL, ML and HL conditions while isotopically nonstationary ^{13}C metabolic flux analysis in Arabidopsis has shown that leaves grown in higher light intensities have lower V_c/V_o (Ma *et al.*, 2014), supporting the idea that

photorespiration could be involved in the dissipation of excess light energy and reducing photodamage (Voss *et al.*, 2013). It should be noted that a detailed quantitative assessment of the TC-ODE-FBA model predictions was not possible because of the lack of soybean-specific data. Comparison of the predicted steady-state metabolite concentrations and organic acid stores against experimental data could help identify additional strengths and weaknesses in the model.

While both models have their advantages and disadvantages, it should be noted that in both LC-ODE-FBA and TC-ODE-FBA set-ups, since the FBA and ODE modules were run separately, the linear and non-linear components of the final models are solved separately. As a result, these models can be solved considerably faster than fully integrated hybrid models, such as the one described by Pozo *et al.* (2015), where the linear and non-linear components have to be solved together as a single non-linear problem. As such the couplings demonstrated in this study, particularly the TC-ODE-FBA model, offer a significant improvement over previously published models of leaf metabolism.

The TC-ODE-FBA model provides a comprehensive description of leaf metabolism

Nocturnal respiration has a significant bearing on the overall change to crop productivity and contradictory data about respiratory responses to high $[CO_2]$ has been reported (Davey *et al.*, 2004, Drake *et al.*, 1999). Both ODE and FBA models on their own are unable to explore such respiratory responses. However, the TC-ODE-FBA model is capable of modelling night-time metabolism under different atmospheric $[CO_2]$ and predicts an increased transitory starch storage and higher night-time respiration with growth under elevated $[CO_2]$. The predicted increase in transitory starch stores in leaves grown in elevated CO_2 agrees with previous experimental observations (Grimmer *et al.*, 1999, Rogers *et al.*, 2004, Ainsworth *et al.*, 2007). Since the FBA model representing night-time metabolism then remobilizes all the transitory starch a higher respiration rate is observed (Fig 6). While this increased rate of night-time respiration is in agreement with published data (Davey *et al.*, 2004), it should be noted that the assumption that all of the transitory starch is remobilized may not always be the case. Grimmer *et al.* (1999) reported that castor bean leaves grown in elevated $[CO_2]$ only partially use up the available starch pool. However data from soy grown using FACE suggests that the leaves are able to use the entire starch pool (Rogers *et al.*, 2004) thus supporting the assumption in the FBA model. Closer inspection of the nocturnal fluxes involving CO_2 in mature leaves showed that while the oxidative pentose-phosphate pathway and pyruvate dehydrogenase are responsible for most of the CO_2 respired, the contribution from tricarboxylic acid (TCA) cycle, malic enzyme and amino acid biosynthesis was also significant (Table 1).

One of the key features of the TC-ODE-FBA model is its ability to use fluxes from the ODE model to predict fluxes through several hundred reactions with relatively little experimental data. Soy-specific gas exchange data was used to parameterise the ODE component. The FBA component of the model required petiole phloem composition (when modelling mature leaves) and leaf biomass composition (when modelling growing leaves). Soy-specific petiole phloem composition data was not available and hence data from tomatoes available in literature was used instead (Supplemental Table S3). Sensitivity analysis was further

performed to demonstrate that the precise phloem composition had negligible impact on the quantitative results discussed in this study (Supplemental Table S9). Soy leaf biomass composition required to model growing soy leaves was experimentally determined (Supplemental Table S2).

To highlight the utility of the model, we also used the TC-ODE-FBA model to compare metabolic fluxes in fully expanded mature leaves and growing leaves. While Fig 7 was used to highlight the differences between the two different modelling scenarios, many differences could not be depicted in Fig 7 owing to these pathways carrying very small fluxes. An example of this is lipid biosynthesis. The TC-ODE-FBA model predicted growing leaves to synthesise phosphatidate at a rate of $2.47 \times 10^{-18} \mu\text{mol.m}^{-2}.\text{s}^{-1}$ during the day (Supplemental Data S7). In other cases, similarities existed between the two scenarios that were not depicted in Fig 7, such as when pathways in the TC-ODE-FBA model did not carry any flux. An example of one such pathway is fatty acid degradation. While fatty acid turnover is likely active in both mature and growing leaves, FBA is incapable of capturing this and hence does not predict fluxes through these pathways. This is also the reason why the mature leaf flux distribution did not predict any lipid biosynthesis. Analysis also showed that the TC-ODE-FBA model predicted a non-cyclic TCA flux in both mature and growing leaves. In both systems, mitochondrial malate dehydrogenase (mMDH) operated in the reverse direction to the conventional TCA cycle, generating malate, which is in agreement with stable isotope labelling studies (Tcherkez *et al.*, 2009, Ma *et al.*, 2014, Xu *et al.*, 2021). This is because photorespiratory flux generates a significant amount of NADH in the mitochondria, which has to be shuttled out into the cytosol via the malate valve (Shameer *et al.*, 2019).

Among the many differences between the two metabolic systems, a significantly higher phosphoenolpyruvate carboxylase (PEPC) activity was predicted in growing leaves. PEPC activity results in the generation of oxaloacetate which can be either reduced to malate, transaminated to aspartate or converted to citrate and then 2-oxoglutarate via the TCA cycle. Growing leaves have a higher protein demand compared to mature leaves and as a result they exhibit increased nitrate uptake and amino acid biosynthesis (Fig. 7). An increased rate of amino acid biosynthesis would generate higher oxaloacetate demands in the system. Anaplerotic C fixation can generate oxaloacetate required for aspartate biosynthesis and this association between PEPC activity and aspartate levels has been previously discussed (Tcherkez and Hodges, 2008). In addition to this, aspartate is also the precursor for lysine, isoleucine and methionine and so the TC-ODE-FBA model predicted increased anaplerotic C fixation in growing leaves. While there is no direct evidence to support this, evidence for positive correlation between N uptake rate and PEPC activity has been reported (Scheible *et al.*, 1997). Besides increased oxaloacetate demands, an increased rate of amino acid biosynthesis would result in increased 2-oxoglutarate demands. Isotopic labelling (^{13}C) studies in leaves have shown that majority of daytime 2-oxoglutarate is generated from metabolites accumulated during the previous night (Gauthier *et al.*, 2010). While 2-oxoglutarate can be generated from citrate stores, it has been shown that this citrate alone is insufficient to meet the leaf's 2-oxoglutarate demands (Tcherkez *et al.*, 2017). Vacuolar aspartate (accumulated in the previous night) has also been proposed as a potential precursor of 2-oxoglutarate and glutamate (Gauthier *et al.*, 2010). While this also points towards a higher night-time PEPC flux under higher day-time amino acid demand, since the TC-ODE-FBA model, (in its current state) was constrained not to accumulate amino acids during the day. Enabling the TC-ODE-FBA model to accumulate additional metabolites in the

vacuole such as sugars and amino acids would potentially improve the ability of these model to capture such complex flux distributions, although with the trade-off of a greater solution space and the potential for non-realistic flux cycling between day and night.

Future development of hybrid ODE-FBA models.

There are many challenges involved in developing hybrid ODE-FBA models (Marshall-Colon *et al.*, 2017), many of which hold true even with ODE and FBA models that model steady-state metabolism. While challenges such as identifying connection points or adjusting for the difference in time scales between models are case-specific, technical challenges such as the difficulty of coupling models running on different platforms and transferring information between models can now be generalized and solved efficiently using cross-platform model integration frameworks such as Yggdrasil (Lang, 2019). While model run-time issues are partly case-specific, the choice for integration framework or platform could help speed up model runs. Yggdrasil uses a python-based environment to execute the individual models, even those native to other platforms, and pass information between them. The availability of fast ODE solvers in MATLAB makes it a good choice to run ODE models. Yggdrasil runs such models, like the e-photosynthesis ODE model, by launching the MATLAB engine via python. This process is time-consuming and was noted to slow down both LC and TC models by a couple of seconds. Nevertheless, Yggdrasil simplifies the process of developing tailored hybrid models, so much so that there is now a strong incentive to enhance FBA models with relevant ODE models and vice-versa.

This study shows how metabolic modelling of C_3 leaves can be improved by coupling ODE and FBA models. Similar advantages of coupling ODE and FBA models are yet to be explored in other plant metabolic systems. As in the case of C_3 photosynthesis described here, kinetic models of C_4 photosynthesis also lack representations for many pathways in primary metabolism (Wang *et al.*, 2014). Coupling such models to FBA models of C_4 leaves (de Oliveira Dal'Molin *et al.*, 2010, Bogart and Myers, 2016) should lead to an improved representation of C_4 metabolism. Storage organs provide another example of a metabolic system which could be better described by tailored hybrid models such as the one described here. FBA models are unable to predict fluxes through futile cycles, an important contributor to metabolic regulation (Claeyssen *et al.*, 2013). ODE models have been shown to be capable of predicting the futile cycling of sucrose in sugarcane (Rowher and Botha 2001, Uys *et al.* 2007). A coupled ODE-FBA model hence has the potential to help the FBA model improve the quality of its predictions by accounting for futile cycles, all the while modelling fluxes through metabolic pathways outside the scope of the ODE models. While ODE based photosynthesis models and diel FBA leaf models have helped improve our understanding of leaf metabolism and have contributed to the development of ideas for metabolic manipulations (Zhu *et al.*, 2007, Cheung *et al.*, 2014, Wang *et al.*, 2014, Cheung *et al.*, 2015, Shameer *et al.*, 2018, Shameer *et al.*, 2019), the higher predictive power and metabolic coverage of the TC model has the potential to further improve upon these ideas and additional applications as illustrated here.

Acknowledgments

Research reported in the publication was supported by the Foundation for Food and Agriculture Research under award number – Grant ID: 602757. The content of this publication is solely the responsibility of the authors and does not necessarily represent the official views of the Foundation for Food and Agriculture Research.

Author contributions

SS and YW developed the coupled models under the supervision of RGR, SPL and LJS, YW collected biological samples; PB performed all biomass estimations; SS, YW, RGR, SPL and LJS wrote the article; all authors approve of the final version of the article for publication.

Conflict of interest

There are no conflicts of interest.

Supplementary files

Supplemental Figure S1 – Estimated V_{cmax_S} and J_{max_S} from A-Ci curves generated by e-photosynthesis model

Supplemental Figure S2 – Models in tightly-coupled configuration achieve convergence within a small number of cycles.

Supplemental Table S1 – Adjusted maximum enzyme activities (V_{max}) in the e-photosynthesis model

Supplemental Table S2 – Soy leaf biomass composition

Supplemental Table S3 – Phloem composition gathered from previously published studies

Supplemental Table S4 – Metabolic constraints for the diel leaf model

Supplemental Table S5 – Relationship between malate and citrate accumulation or remobilization fluxes and starch accumulation flux in diel FBA model

Supplemental Table S6 – Metabolic constraints for single phase day-time model

Supplemental Table S7 – Metabolic constraints for single phase night-time model

Supplemental Table S8 – A comparison of the capabilities of ODE, FBA, LC-ODE-FBA and Tc-ODE-FBA models

Supplemental Table S9 – Sensitivity analysis of TC-ODE-FBA model parameters

Supplemental Information S1 – Evaluating the sensitivity of tightly-coupled ODE-FBA model (TC-ODE-FBA) results to model parameters.

Supplemental Data S1 – Updates to PlantCoreMetabolism v1.2.0

Supplemental Data S2 – Flux distribution for FACE conditions predicted by LC-ODE-FBA model

Supplemental Data S3 – Flux distribution for FACE conditions predicted by ODE model

Supplemental Data S4 – Flux distribution for FACE conditions predicted by FBA model

Supplemental Data S5 – Flux distribution for FACE conditions predicted by TC-ODE-FBA model

Supplemental Data S6 – Daytime flux distributions for LL, ML, HL and HL-E conditions predicted by the TC-ODE-FBA model

Supplemental Data S7 – Flux distribution in mature and growing leaves predicted by TC-ODE-FBA model

References

- Ainsworth, E.A., Rogers, A., Leakey, A.D., Heady, L.E., Gibon, Y., Stitt, M. and Schurr, U. (2007) Does elevated atmospheric [CO₂] alter diurnal C uptake and the balance of C and N metabolites in growing and fully expanded soybean leaves? *Journal of Experimental Botany*, **58**, 579-591.
- Arnold, A. and Nikoloski, Z. (2014) Bottom-up metabolic reconstruction of Arabidopsis and its application to determining the metabolic costs of enzyme production. *Plant Physiology*, **165**, 1380-1391.
- Beard, D.A. and Qian, H. (2005) Constraint-based modeling of metabolomic systems. In *Encyclopedia of Genetics, Genomics, Proteomics and Bioinformatics* (Vol. 3). John Wiley and Sons, Ltd.
- Bernacchi, C.J., Morgan, P.B., Ort, D.R. and Long, S.P. (2005) The growth of soybean under free air [CO₂] enrichment (FACE) stimulates photosynthesis while decreasing *in vivo* Rubisco capacity. *Planta*, **220**, 434-446.
- Bogart, E. and Myers, C.R. (2016) Multiscale metabolic modeling of C4 plants: connecting nonlinear genome-scale models to leaf-scale metabolism in developing maize leaves. *PLoS ONE*, **11**, e0151722.
- Canarini, A., Merchant, A., & Dijkstra, F. A. (2016). Drought effects on *Helianthus annuus* and *Glycine max* metabolites: from phloem to root exudates. *Rhizosphere*, **2**, 85–97.
- Chatterjee, A., Huma, B., Shaw, R. and Kundu, S. (2017) Reconstruction of *Oryza sativa indica* genome scale metabolic model and its responses to varying rubisco activity, light intensity, and enzymatic cost conditions. *Frontiers in Plant Science*, **8**, 2060.
- Cheung, C.M., Poolman, M.G., Fell, D.A., Ratcliffe, R.G. and Sweetlove, L.J. (2014) A diel flux balance model captures interactions between light and dark metabolism during day-night cycles in C₃ and crassulacean acid metabolism leaves. *Plant Physiology*, **165**, 917-929.
- Cheung, C.M., Ratcliffe, R.G. and Sweetlove, L.J. (2015) A method of accounting for enzyme costs in flux balance analysis reveals alternative pathways and metabolite stores in an illuminated Arabidopsis leaf. *Plant Physiology*, **169**, 1671-1682.
- Claeysen, É., Dorion, S., Clendenning, A., He, J. Z., Wally, O., Chen, J., Auslender, E. L., Moisan, M.-C., Jolicoeur, M., and Rivoal, J. (2013) The futile cycling of hexose phosphates could account for the fact that hexokinase exerts a high control on glucose phosphorylation but not on glycolytic rate in transgenic potato (*Solanum tuberosum*) roots. *PLoS ONE*, **8**, e53898.
- Cox, P., Betts, R., Bunton, C., Essery, R., Rowntree, P. and Smith, J. (1999) The impact of new land surface physics on the GCM simulation of climate and climate sensitivity. *Climate Dynamics*, **15**, 183-203.
- Davey, P.A., Hunt, S., Hymus, G.J., DeLucia, E.H., Drake, B.G., Karnosky, D.F. and Long, S.P. (2004) Respiratory oxygen uptake is not decreased by an instantaneous elevation of [CO₂], but is increased with long-term growth in the field at elevated [CO₂]. *Plant Physiology*, **134**, 520-527.
- de Oliveira Dal'Molin, C.G., Quek, L.-E., Palfreyman, R.W., Brumbley, S.M. and Nielsen, L.K. (2010) AraGEM, a genome-scale reconstruction of the primary metabolic network in Arabidopsis. *Plant Physiology*, **152**, 579-589.
- de Oliveira Dal'Molin, C.G., Quek, L.-E., Palfreyman, R.W., Brumbley, S.M. and Nielsen, L.K. (2010) C4GEM, a genome-scale metabolic model to study C₄ plant metabolism. *Plant Physiology*, **154**, 1871-1885.

- Drake, B.G., Azcon - Bieto, J., Berry, J., Bunce, J., Dijkstra, P., Farrar, J., Gifford, R., Gonzalez - Meler, M., Koch, G. and Lambers, H. (1999) Does elevated atmospheric CO₂ concentration inhibit mitochondrial respiration in green plants? *Plant, Cell & Environment*, **22**, 649-657.
- Farquhar, G.D., von Caemmerer, S. and Berry, J. (1980) A biochemical model of photosynthetic CO₂ assimilation in leaves of C₃ species. *Planta*, **149**, 78-90.
- Fridlyand, L.E. and Scheibe, R. (1999) Regulation of the Calvin cycle for CO₂ fixation as an example for general control mechanisms in metabolic cycles. *Biosystems*, **51**, 79-93.
- Fujihara, S., Yamamoto, K., & Yamaguchi, M. (1977) A possible role of allantoin and the influence of nodulation on its production in soybean plants. *Plant and Soil*, **48**, 233–242.
- Gauthier, P. P. G., Bligny, R., Gout, E., Mahé, A., Nogués, S., Hodges, M., and Tcherkez, G. G. B. (2010). *In folio* isotopic tracing demonstrates that nitrogen assimilation into glutamate is mostly independent from current CO₂ assimilation in illuminated leaves of *Brassica napus*. *New Phytologist*, **185**(4), 988–999.
- Gombert, A.K. and Nielsen, J. (2000) Mathematical modelling of metabolism. *Current Opinion in Biotechnology*, **11**, 180-186.
- Grafahrend-Belau, E., Junker, A., Eschenröder, A., Müller, J., Schreiber, F. and Junker, B.H. (2013) Multiscale metabolic modeling: dynamic flux balance analysis on a whole-plant scale. *Plant Physiology*, **163**, 637-647.
- Grimmer, C., Bachfischer, T. and Komor, E. (1999) Carbohydrate partitioning into starch in leaves of *Ricinus communis* L. grown under elevated CO₂ is controlled by sucrose. *Plant, Cell & Environment*, **22**, 1275-1280.
- Haile, F.J. and Higley, L.G. (2003) Changes in soybean gas-exchange after moisture stress and spider mite injury. *Environmental Entomology*, **32**, 433-440.
- Heckmann, D., Schulze, S., Denton, A., Gowik, U., Westhoff, P., Weber, A.P. and Lercher, M.J. (2013) Predicting C₄ photosynthesis evolution: modular, individually adaptive steps on a Mount Fuji fitness landscape. *Cell*, **153**, 1579-1588.
- Herrmann, H.A., Dyson, B.C., Vass, L., Johnson, G.N. and Schwartz, J.-M. (2019) Flux sampling is a powerful tool to study metabolism under changing environmental conditions. *NPJ Systems Biology and Applications*, **5**, 1-8.
- Hooper, C. M., Castleden, I. R., Aryamanesh, N., Jacoby, R. P., & Millar, A. H. (2016) Finding the subcellular location of barley, wheat, rice and maize proteins: the compendium of crop proteins with annotated locations (cropPAL). *Plant and Cell Physiology*, **57**, e9(1–9).
- Imam, S., Schäuble, S., Valenzuela, J., López García de Lomana, A., Carter, W., Price, N.D. and Baliga, N.S. (2015) A refined genome - scale reconstruction of *Chlamydomonas* metabolism provides a platform for systems - level analyses. *The Plant Journal*, **84**, 1239-1256.
- Kamsen, R., Kalapanulak, S., Chiewchankaset, P. and Saithong, T. (2021) Transcriptome integrated metabolic modeling of carbon assimilation underlying storage root development in cassava. *Scientific Reports*, **11**, 8758.
- Kleessen, S., Irgang, S., Klie, S., Giavalisco, P. and Nikoloski, Z. (2015) Integration of transcriptomics and metabolomics data specifies the metabolic response of *Chlamydomonas* to rapamycin treatment. *The Plant Journal*, **81**, 822-835.
- Kleessen, S. and Nikoloski, Z. (2012) Dynamic regulatory on/off minimization for biological systems under internal temporal perturbations. *BMC Systems Biology*, **6**, 16.
- Kromdijk, J., Glowacka, K., Leonelli, L., Gabilly, S.T., Iwai, M., Niyogi, K.K. and Long, S.P. (2016) Improving photosynthesis and crop productivity by accelerating recovery from photoprotection. *Science*, **354**, 857-861.
- Laisk, A., Eichelmann, H., Oja, V., Eatherall, A. and Walker, D.A. (1989) A mathematical model of the carbon metabolism in photosynthesis. Difficulties in explaining oscillations by fructose 2, 6-bisphosphate regulation. *Proceedings of the Royal Society of London. B. Biological Sciences*, **237**, 389-415.

- Laisk, A. and Walker, D.A.** (1986) Control of phosphate turnover as a rate-limiting factor and possible cause of oscillations in photosynthesis: a mathematical model. *Proceedings of the Royal society of London. Series B. Biological sciences*, **227**, 281-302.
- Lakshmanan, M., Lim, S.-H., Mohanty, B., Kim, J.K., Ha, S.-H. and Lee, D.-Y.** (2015) Unraveling the light-specific metabolic and regulatory signatures of rice through combined in silico modeling and multiomics analysis. *Plant Physiology*, **169**, 3002-3020.
- Lang, M.** (2019) yggdrasil: a Python package for integrating computational models across languages and scales. *in silico Plants*, **1**, diz001.
- Laurens, L.M., Quinn, M., Van Wycken, S., Templeton, D.W. and Wolfrum, E.J.** (2012) Accurate and reliable quantification of total microalgal fuel potential as fatty acid methyl esters by in situ transesterification. *Analytical and Bioanalytical Chemistry*, **403**, 167-178.
- Lisec, J., Schauer, N., Kopka, J., Willmitzer, L. and Fernie, A.R.** (2006) Gas chromatography mass spectrometry-based metabolite profiling in plants. *Nature Protocols*, **1**, 387-396.
- Long, C.P. and Antoniewicz, M.R.** (2014) Quantifying biomass composition by gas chromatography/mass spectrometry. *Analytical chemistry*, **86**, 9423-9427.
- Long, S., Burgess, S. and Causton, I.** (2019) Redesigning crop photosynthesis. *Sustaining Global Food Security: The Nexus of Science and Policy* (Zeigler R., eds), Canberra: CSIRO Publishing, pp 61-144.
- López-Calcano, P.E., Brown, K.L., Simkin, A.J., Fisk, S.J., Violet-Chabrand, S., Lawson, T. and Raines, C.A.** (2020) Stimulating photosynthetic processes increases productivity and water-use efficiency in the field. *Nature Plants*, **6**, 1054-1063.
- Ma, F., Jazmin, L.J., Young, J.D. and Allen, D.K.** (2014) Isotopically nonstationary ^{13}C flux analysis of changes in *Arabidopsis thaliana* leaf metabolism due to high light acclimation. *Proceedings of the National Academy of Sciences*, **111**, 16967-16972.
- Marshall-Colon, A., Long, S.P., Allen, D.K., Allen, G., Beard, D.A., Benes, B., Von Caemmerer, S., Christensen, A., Cox, D.J. and Hart, J.C.** (2017) Crops *in silico*: generating virtual crops using an integrative and multi-scale modeling platform. *Frontiers in Plant Science*, **8**, 786.
- McGrath JM, Long SP** (2014) Can the cyanobacterial carbon-concentrating mechanism increase photosynthesis in crop species? A theoretical analysis. *Plant Physiology*, **164**, 2247-2261.
- Miguez, F.E., Zhu, X., Humphries, S., Bollero, G.A. and Long, S.P.** (2009) A semimechanistic model predicting the growth and production of the bioenergy crop *Miscanthus x giganteus*: description, parameterization and validation. *GCB Bioenergy*, **1**, 282-296.
- Mintz-Oron, S., Meir, S., Malitsky, S., Ruppin, E., Aharoni, A. and Shlomi, T.** (2012) Reconstruction of Arabidopsis metabolic network models accounting for subcellular compartmentalization and tissue-specificity. *Proceedings of the National Academy of Sciences*, **109**, 339-344.
- Miyake, C., Miyata, M., Shinzaki, Y., & Tomizawa, K.** (2005). CO_2 response of cyclic electron flow around PSI (CEF-PSI) in tobacco leaves—Relative electron fluxes through PSI and PSII determine the magnitude of non-photochemical quenching (NPQ) of Chl fluorescence. *Plant and Cell Physiology*, **46**, 629-637.
- Morales, A., Yin, X., Harbinson, J., Driever, S.M., Molenaar, J., Kramer, D.M. and Struik, P.C.** (2018) In silico analysis of the regulation of the photosynthetic electron transport chain in C_3 plants. *Plant Physiology*, **176**, 1247-1261.
- Morgan, P.B., Bernacchi, C.J., Ort, D.R. and Long, S.P.** (2004) An in vivo analysis of the effect of season-long open-air elevation of ozone to anticipated 2050 levels on photosynthesis in soybean. *Plant Physiology*, **135**, 2348-2357.

- Niño-González, M., Novo-Uzal, E., Richardson, D. N., Barros, P. M., & Duque, P.** (2019) More transporters, more substrates: the Arabidopsis major facilitator superfamily revisited. *Molecular Plant*, **12**, 1182–1202.
- Nicol, L., Nawrocki, W. J., & Croce, R.** (2019). Disentangling the sites of non-photochemical quenching in vascular plants. *Nature Plants*, **5**, 1177–1183.
- Orth, J.D., Thiele, I. and Palsson, B.Ø.** (2010) What is flux balance analysis? *Nature Biotechnology*, **28**, 245-248.
- Paul, M.J. and Foyer, C.H.** (2001) Sink regulation of photosynthesis. *Journal of Experimental Botany*, **52**, 1383-1400.
- Paul, M.J. and Pellny, T.K.** (2003) Carbon metabolite feedback regulation of leaf photosynthesis and development. *Journal of Experimental Botany*, **54**, 539-547.
- Pearcy, R., Gross, L. and He, D.** (1997) An improved dynamic model of photosynthesis for estimation of carbon gain in sunfleck light regimes. *Plant, Cell & Environment*, **20**, 411-424.
- Poolman, M.G., Fell, D.A. and Thomas, S.** (2000) Modelling photosynthesis and its control. *Journal of Experimental Botany*, **51**, 319-328.
- Poolman, M.G., Kundu, S., Shaw, R. and Fell, D.A.** (2013) Responses to light intensity in a genome-scale model of rice metabolism. *Plant Physiology*, **162**, 1060-1072.
- Poolman, M.G., Miquet, L., Sweetlove, L.J. and Fell, D.A.** (2009) A genome-scale metabolic model of Arabidopsis and some of its properties. *Plant Physiology*, **151**, 1570-1581.
- Pozo, C., Miró, A., Guillén-Gosálbez, G., Sorribas, A., Alves, R. and Jiménez, L.** (2015) Global optimization of hybrid kinetic/FBA models via outer-approximation. *Computers & Chemical Engineering*, **72**, 325-333.
- Pries, C., Razaghi-Moghadam, Z., Kopka, J. and Nikoloski, Z.** (2021) Integration of relative metabolomics and transcriptomics time-course data in a metabolic model pinpoints effects of ribosome biogenesis defects on Arabidopsis thaliana metabolism. *Scientific Reports*, **11**, 4787.
- Rahimzadeh-Bajgiran, P., Tubuxin, B., & Omasa, K.** (2017). Estimating chlorophyll fluorescence parameters using the joint Fraunhofer line depth and laser-induced saturation pulse (FLD-LISP) method in different plant species. *Remote Sensing*, **9**.
- Recht, L., Töpfer, N., Batushansky, A., Sikron, N., Gibon, Y., Fait, A., Nikoloski, Z., Boussiba, S. and Zarka, A.** (2014) Metabolite profiling and integrative modeling reveal metabolic constraints for carbon partitioning under nitrogen starvation in the green algae *Haematococcus pluvialis*. *Journal of Biological Chemistry*, **289**, 30387-30403.
- Rogers, A., Allen, D., Davey, P., Morgan, P., Ainsworth, E., Bernacchi, C., Cornic, G., Dermody, O., Dohleman, F. and Heaton, E.** (2004) Leaf photosynthesis and carbohydrate dynamics of soybeans grown throughout their life-cycle under free-air carbon dioxide enrichment. *Plant, Cell & Environment*, **27**, 449-458.
- Sajitz-Hermstein, M., Töpfer, N., Kleessen, S., Fernie, A.R. and Nikoloski, Z.** (2016) iReMet-flux: constraint-based approach for integrating relative metabolite levels into a stoichiometric metabolic models. *Bioinformatics*, **32**, i755-i762.
- Scheible, W.-R., Gonzalez-Fontes, A., Lauerer, M., Muller-Rober, B., Caboche, M. and Stitt, M.** (1997) Nitrate acts as a signal to induce organic acid metabolism and repress starch metabolism in tobacco. *The Plant Cell*, **9**, 783-798.
- Scheunemann, M., Brady, S.M. and Nikoloski, Z.** (2018) Integration of large-scale data for extraction of integrated Arabidopsis root cell-type specific models. *Scientific reports*, **8**, 7919.
- Schroeder, W.L. and Saha, R.** (2020) Introducing an optimization- and explicit Runge-Kutta-based approach to perform dynamic flux balance analysis. *Scientific reports*, **10**, 9241.
- Sellers, P.J., Tucker, C.J., Collatz, G.J., Los, S.O., Justice, C.O., Dazlich, D.A. and Randall, D.A.** (1996) A revised land surface parameterization (SiB2) for atmospheric

- GCMs. Part II: The generation of global fields of terrestrial biophysical parameters from satellite data. *Journal of Climate*, **9**, 706-737.
- Shameer, S., Baghalian, K., Cheung, C.M., Ratcliffe, R.G. and Sweetlove, L.J.** (2018) Computational analysis of the productivity potential of CAM. *Nature Plants*, **4**, 165-171.
- Shameer, S., Ratcliffe, R.G. and Sweetlove, L.J.** (2019) Leaf energy balance requires mitochondrial respiration and export of chloroplast NADPH in the light. *Plant Physiology*, **180**, 1947-1961.
- Shameer, S., Vallarino, J.G., Fernie, A.R., Ratcliffe, R.G. and Sweetlove, L.J.** (2020) Flux balance analysis of metabolism during growth by osmotic cell expansion and its application to tomato fruits. *The Plant Journal*, **103**, 68-82.
- Shaw, R. and Cheung, C.** (2018) A dynamic multi-tissue flux balance model captures carbon and nitrogen metabolism and optimal resource partitioning during *Arabidopsis* growth. *Frontiers in Plant Science*, **9**, 884.
- Simons, M., Saha, R., Amiour, N., Kumar, A., Guillard, L., Clément, G., Miquel, M., Li, Z., Mouille, G. and Lea, P.J.** (2014) Assessing the metabolic impact of nitrogen availability using a compartmentalized maize leaf genome-scale model. *Plant Physiology*, **166**, 1659-1674.
- Siriwach, R., Matsuda, F., Yano, K. and Hirai, M.Y.** (2020) Drought stress responses in context-specific genome-scale metabolic models of *Arabidopsis thaliana*. *Metabolites*, **10**, 159.
- South, P.F., Cavanagh, A.P., Liu, H.W. and Ort, D.R.** (2019) Synthetic glycolate metabolism pathways stimulate crop growth and productivity in the field. *Science*, **363**, eaat9077.
- Sun, J., Feng, Z., Leakey, A.D., Zhu, X., Bernacchi, C.J. and Ort, D.R.** (2014) Inconsistency of mesophyll conductance estimate causes the inconsistency for the estimates of maximum rate of Rubisco carboxylation among the linear, rectangular and non-rectangular hyperbola biochemical models of leaf photosynthesis—A case study of CO₂ enrichment and leaf aging effects in soybean. *Plant Science*, **226**, 49-60.
- Takagi, H., Watanabe, S., Tanaka, S., Matsuura, T., Mori, I. C., Hirayama, T., Shimada, H., and Sakamoto, A.** (2018) Disruption of ureide degradation affects plant growth and development during and after transition from vegetative to reproductive stages. *BMC Plant Biology*, **18**, 287.
- Tcherkez, G., & Hodges, M.** (2008). How stable isotopes may help to elucidate primary nitrogen metabolism and its interaction with (photo)respiration in C₃ leaves. *Journal of Experimental Botany*, **59**, 1685–1693.
- Tcherkez, G., Mahé, A., Gauthier, P., Mauve, C., Gout, E., Bligny, R., Cornic, G. and Hodges, M.** (2009) In folio respiratory fluxomics revealed by ¹³C isotopic labeling and H/D isotope effects highlight the noncyclic nature of the tricarboxylic acid “cycle” in illuminated leaves. *Plant Physiology*, **151**, 620-630.
- Tcherkez, G., Gauthier, P., Buckley, T. N., Busch, F. A., Barbour, M. M., Bruhn, D., Heskell, M. A., Gong, X. Y., Crous, K. Y., Griffin, K., Way, D., Turnbull, M., Adams, M. A., Atkin, O. K., Farquhar, G. D., & Cornic, G.** (2017). Leaf day respiration: low CO₂ flux but high significance for metabolism and carbon balance. *New Phytologist*, **216**, 986–1001.
- Töpfer, N., Braam, T., Shameer, S., Ratcliffe, R. G., & Sweetlove, L. J.** (2020). Alternative CAM modes provide environment-specific water-saving benefits in a leaf metabolic model. *The Plant Cell*, **32**, 3689-3705.
- Traub, M., Flörchinger, M., Piecuch, J., Kunz, H. H., Weise-Steinmetz, A., Deitmer, J. W., Neuhaus, H. E., & Möhlmann, T.** (2007) The fluorouridine insensitive 1 (*fur1*) mutant is defective in equilibrative nucleoside transporter 3 (ENT3), and thus represents an important pyrimidine nucleoside uptake system in *Arabidopsis thaliana*. *The Plant Journal*, **49**, 855–864.

- Valle, E.M., Boggio, S.B. and Heldt, H.W.** (1998) Free amino acid composition of phloem sap and growing fruit of *Lycopersicon esculentum*. *Plant and Cell Physiology*, **39**, 458-461.
- von Caemmerer, S.** (2000) *Biochemical models of leaf photosynthesis*. CSIRO Publishing.
- Vos, J., Evers, J.B., Buck-Sorlin, G.H., Andrieu, B., Chelle, M. and De Visser, P.H.** (2010) Functional–structural plant modelling: a new versatile tool in crop science. *Journal of Experimental Botany*, **61**, 2101-2115.
- Voss, I., Sunil, B., Scheibe, R., & Raghavendra, A. S.** (2013). Emerging concept for the role of photorespiration as an important part of abiotic stress response. *Plant Biology*, **15**, 713–722.
- Walker, A. and Ho, L.** (1977) Carbon translocation in the tomato: carbon import and fruit growth. *Annals of Botany*, **41**, 813-823.
- Wang, Y., Long, S.P. and Zhu, X.-G.** (2014) Elements required for an efficient NADP-malic enzyme type C₄ photosynthesis. *Plant Physiology*, **164**, 2231-2246.
- Woodrow, I.E. and Mott, K.A.** (1993) Modelling C₃ photosynthesis: A sensitivity analysis of the photosynthetic carbon-reduction cycle. *Planta*, **191**, 421-432.
- Xu, Y., Fu, X., Sharkey, T. D., Shachar-Hill, Y., & Walker, B. J.** (2021) The metabolic origins of non-photorespiratory CO₂ release during photosynthesis: A metabolic flux analysis. *Plant Physiology*, **58**, 7250–7257.
- Yao, X., Zhou, H., Zhu, Q., Li, C., Zhang, H., Wu, J.-J. and Xie, F.** (2017) Photosynthetic response of soybean leaf to wide light-fluctuation in maize-soybean intercropping system. *Frontiers in Plant Science*, **8**, 1695.
- Yin, X. and Struik, P.** (2009) C₃ and C₄ photosynthesis models: An overview from the perspective of crop modelling. *NJAS-Wageningen Journal of Life Sciences*, **57**, 27-38.
- Yoon, D.-K., Ishiyama, K., Suganami, M., Tazoe, Y., Watanabe, M., Imaruoka, S., Ogura, M., Ishida, H., Suzuki, Y. and Obara, M.** (2020) Transgenic rice overproducing Rubisco exhibits increased yields with improved nitrogen-use efficiency in an experimental paddy field. *Nature Food*, **1**, 134-139.
- Yuan, H., Cheung, C.M., Poolman, M.G., Hilbers, P.A. and van Riel, N.A.** (2016) A genome - scale metabolic network reconstruction of tomato (*Solanum lycopersicum* L.) and its application to photorespiratory metabolism. *The Plant Journal*, **85**, 289-304.
- Zaks, J., Amarnath, K., Kramer, D.M., Niyogi, K.K. and Fleming, G.R.** (2012) A kinetic model of rapidly reversible nonphotochemical quenching. *Proceedings of the National Academy of Sciences*, **109**, 15757-15762.
- Zhang, Y.-L., Hu, Y.-Y., Luo, H.-H., Chow, W.S. and Zhang, W.-F.** (2011) Two distinct strategies of cotton and soybean differing in leaf movement to perform photosynthesis under drought in the field. *Functional Plant Biology*, **38**, 567-575.
- Zhao, H.-L., Chang, T.G., Xiao, Y. and Zhu, X.-G.** (2021) Potential metabolic mechanisms for inhibited chloroplast nitrogen assimilation under high CO₂. *Plant Physiology*, in press.
- Zhu, X.-G., De Sturler, E. and Long, S.P.** (2007) Optimizing the distribution of resources between enzymes of carbon metabolism can dramatically increase photosynthetic rate: a numerical simulation using an evolutionary algorithm. *Plant Physiology*, **145**, 513-526.
- Zhu, X.-G., Long, S.P. and Ort, D.R.** (2008) What is the maximum efficiency with which photosynthesis can convert solar energy into biomass? *Current Opinion in Biotechnology*, **19**, 153-159.
- Zhu, X.-G., Long, S.P. and Ort, D.R.** (2010) Improving photosynthetic efficiency for greater yield. *Annual Review of Plant Biology*, **61**, 235-261.
- Zhu, X.G., Wang, Y., Ort, D.R. and Long, S.P.** (2013) e-photosynthesis: a comprehensive dynamic mechanistic model of C₃ photosynthesis: from light capture to sucrose synthesis. *Plant, Cell & Environment*, **36**, 1711-1727.

